/afcs

CERN/MPS/LIN 74-1
6.9.1974

DESIGN OF THE LOW ENERGY BEAM TRANSPORT SYSTEM FOR THE NEW 50 MeV LINAC

B. Bru and M. Weiss

SUMMARY

The design of the low energy beam transport system (LEBT) for the new 50 MeV Linac is analysed in particular from the beam optical point of view. Principles and methods on which the design has been based are reported.

A six-dimensional matching to the Linac input is ensured for all envisaged Linac operating conditions and for beam intensities of up to 250 mA. The mean beam diameter at injection to the Linac can be kept smaller than 8 mm. With wider beams, higher intensities than 250 mA may be injected. About 80% of the injected beam is trapped into the Linac acceptance, particularly due to a bunching system composed of three bunchers.

The LEBT is equipped in several places with beam measuring apparatus, electron traps and also a system, which can limit the beam proportionally in diameter and divergence.

The optimized LEBT design has been obtained by leaning heavily on a specially developed approach, which, in turn, made use of linear and multi-particle computer programs, developed or improved at CERN over the past five years.

CONTENTS

1. INTRODUCTION - BASIC PHILOSOPHY

The present paper deals with the design of the low energy beam transport system (LEBT), emphasizing the methods by which the beam dynamics in this part of the new Linac complex has been optimized.

The task of LEBT is to transport the pre-accelerator beam and to match it to the Linac acceptance with as high a trapping efficiency as possible. The Linac acceptance is defined in six-dimensional phase space and is a function of Linac settings as well as of the beam to be accelerated ; the high trapping efficiency is needed in order that the non-trapped, but still present particles do not disturb the beam dynamics in the first Linac tank.

The LEBT has for convenience been divided into several sections, which were at first analysed separately. Apart from transporting the beam, each section has been assigned a particular task, for example to measure the beam characteristics or to limit its intensity in an appropriate way. Some sections contain empty drift spaces, foreseen for a later inclusion of apparatus (a 3 MHz chopper or a bending magnet at the junction with a possible H^- beam line). The most important section is the last one, the bunching section, where the transition from a continuous to a bunched beam takes place and where the six-dimensional matching to the Linac input is ensured.

The basic philosophy adopted for the LEBT design (and concerning in particular the bunching section) has been to treat the problem first by a specially developed method, which made use of linear optimisation routines ; the results were successively checked by a multiparticle program and modifications made in the design where necessary. The combined use of these two approaches was beneficial for the understanding of several important phenomena in the LEBT as well as for the assurance that trapping efficiencies of the order of 80% could be achieved (when quoting trapping efficiency, one refers always to the one obtained by the multiparticle program).

2. PRE-ACCELERATOR BEAM CHARACTERISTICS - RMS VALUES

The input conditions relevant to the design of LEBT are the characteristics of the pre-accelerator beam at 750keV. These characteristics are not known yet, but a reasonable guess can be made, based on the knowledge of our present 500keV beam and on properties of 750keV beam at other laboratories such as NAL and BNL.

For design purposes, a beam is conveniently described by the intensity and by the second momenta of its coordinates in phase space. Provided the density distribution in the beam is of the ellipsoidal type, the evolution of the second momenta during beam transport depends only on the linear component of space charge forces[1]. Hence, dealing with rms values of coordinates rather than with marginal ones, one makes possible the use of linear optimisation programs in beam transport problems.

Beams with different density distributions, but with the same second momenta of phase space coordinates require practically the same settings of matching elements*). One has therefore optimised the matching for an "equivalent" beam having the required second momenta and a uniform density distribution in real space, which automatically gives rise to linear space charge forces.

The characteristics of the nominal, equivalent beam at input to the LEBT(cathode of the 750 kV DC accelerating column) are chosen as :

Beam intensity (mA)	200	
	Marginal value	rms value
Transverse emittance, unnormalised (m rad)	$E_x = E_y = 65\ 10^{-6}$	$E_{xrms} = E_{yrms} = 16.25\ 10^{-6}$
Beam envelope (mm)	$\hat{x} = \hat{y} = 10$	$\tilde{x} = \tilde{y} = 5$ ($\tilde{x},\tilde{y}$ stand for $\sqrt{\overline{x^2}}$, $\sqrt{\overline{y^2}}$)
Beam divergence (rad) (defocused beam)	$\hat{x}' = \hat{y}' = 25\ 10^{-3}$	$\tilde{x}' = \tilde{y}' = 12.5\ 10^{-3}$

*) This statement is not fully verified for the buncher settings, see section 4 and Appendix II.

Defining the beam with its marginal and rms coordinates, one has also given information about the density distribution (another way of defining would be with either the marginal or rms coordinates and the density distribution). The relations between the rms and marginal values are :

$\hat{x} = k\tilde{x}$ and analogously for $\hat{x}'$, $\hat{y}$ and $\hat{y}'$;

$E_x = k^2 E_{xrms}$ and analogously for E_y ;

The factor k depends on the density distribution. The formula for the rms emittance contains the second momenta of the distribution and is written as :

$$E_{xrms} = \left[\overline{x^2}\ \overline{x'^2} - (\overline{xx'})^2 \right]^{\frac{1}{2}}$$

In Appendix 1, one has assembled some useful formulae relating rms and marginal values for some typical density distributions.

3. SYSTEM FOR BEAM LIMITATION

The output beam intensity of the new linac has to be variable in the range of 50 to 150 mA[2]. To achieve this, one intends to have three means at our disposition :

i) changing the ion source settings,

ii) changing the linac settings,

iii) introducing limiting apertures.

A convenient system of apertures, which can limit the beam proportionally in diameter and divergence is introduced in the early part of the LEBT.

The conditions to be fulfilled by a system of two 4-jaw apertures can be derived with the help of Fig. 2a :

The equation of the marginal emittance ellipse in a transverse phase plane at aperture AP1 is :

$$\frac{\overline{x'^2}}{E_{rms}} x^2 - 2\frac{\overline{xx'}}{E_{rms}} xx' + \frac{\overline{x^2}}{E_{rms}} x'^2 = E \qquad *)$$

The tangent at point P_{11} (see Fig. 2a) has the equation :

$$x'_1 = \frac{\overline{xx'_1}}{\overline{x_1^2}} x_1 + \frac{kE_{rms}}{\tilde{x}_1} \text{ , where } k = \left(\frac{E}{E_{rms}}\right)^{\frac{1}{2}}.$$

This tangent should become a vertical line at AP2

$$x_2 = t_{11}x_1 + t_{12}x'_1$$

(t_{11}, t_{12} ... elements of the transfer matrix).

The point P_{11} transforms into P_{21} :

$$x_{21} = t_{12} \frac{kE_{rms}}{\tilde{x}_1}$$

The point P_{12} transforms into P_{22} :

$$x_{22} = -t_{11}\, kE_{rms} \frac{\tilde{x}_1}{\overline{x_1 x'_1}}$$

---

*) It is more logical to write the formula of the ellipse with the rms values of phase space coordinates, rather than with the usual parameters α, β, γ; the relation between the two definitions is :

$$\begin{pmatrix} \beta & -\alpha \\ -\alpha & \gamma \end{pmatrix} = \frac{1}{E_{rms}} \begin{pmatrix} \overline{x^2} & \overline{xx'} \\ \overline{xx'} & \overline{x'^2} \end{pmatrix}$$

As $x_{21} = x_{22}$, the condition for the transfer matrix elements of the beam limiting system is :

$$\frac{t_{11}}{t_{12}} = -\frac{\overline{x_1 x_1'}}{\overline{x_1^2}} \qquad (1)$$

It has been found that the most suitable beam limiting system is the one not containing any lenses between apertures AP1 and AP2 ; the condition (1) is fulfilled with lenses preceding AP1. At AP1 one must obviously have a focusing beam, see Fig. 2b. Additional conditions can be derived from Fig. 2b :

Beam envelope at AP2 (transformation of point P_{11}) :

$$\hat{x}_2 = k\tilde{x}_2 = t_{12}\frac{kE_{rms}}{\tilde{x}_1} \rightarrow \underline{t_{12} = \frac{\tilde{x}_1\tilde{x}_2}{E_{rms}}} \qquad (2)$$

Formulae (1) and (2) are general and apply also if space charge (linear forces) is taken into account. Other useful "guiding" formulae, but valid only for zero space charge, can be obtained from Fig. 2b :

Distance L between AP1 and AP2 (transformation of P_{11} to P_{21}) :

$$x_{11}' \cdot L = \frac{kE_{rms}}{\tilde{x}_1} L = -kE_{rms}\frac{\tilde{x}_1}{\overline{x_1 x_1'}} \rightarrow \underline{L = -\frac{\overline{x_1^2}}{\overline{x_1 x_1'}}} \qquad (3)$$

Relation between beam envelopes $\hat{x}_1$ and $\hat{x}_2$ (point P_{13} and P_{21}) :

$$\hat{x}_1 = k\tilde{x}_1 \quad ; \quad \hat{x}_2 = -kE_{rms}\frac{\tilde{x}_1}{\overline{x_1 x_1'}} \qquad \underline{\frac{\hat{x}_2}{\hat{x}_1} = -\frac{E_{rms}}{\overline{x_1 x_1'}}} \qquad (4)$$

Between AP1 and AP2 the beam has a neck ; the beam radius at the neck is (point P_{14}) :

$$a = \frac{kE_{rms}}{\tilde{x}'_1} \qquad (5)$$

The position of the neck L_n is (transformation of point P_{15}) :

$$x'_{15}\ L_n = k\,\tilde{x}'_1 \,.\, L_n = -\,k\,\frac{\overline{x_1 x'_1}}{\tilde{x}'_1} \rightarrow \underline{L_n = -\,\frac{\overline{x_1 x'_1}}{x'^2_1}}\ , \qquad (6)$$

or related to the distance between AP1 and AP2 :

$$\frac{L_n}{L} = \frac{(\overline{x_1 x'_1})^2}{\overline{x_1^2}\,\overline{x'^2_1}} \qquad (7)$$

The formulae (1) to (7) determine, in principle, a beam limiting system. In practice, the design has to include other constraints for example, the choice of an appropriate distance between apertures and a check that the beam sizes and divergences at and between AP1 and AP2 are of reasonable values ; this has to be verified for all beam intensities in the region of interest.

A computer program, CTBEAM[3], has been written and used to analyse beam limiting systems. The results of calculations are presented in Fig. 3 in the form :

$L = f\left(\frac{\overline{x_1 x'_1}}{E_{rms}}\right)$, with $\frac{\overline{x_1^2}}{E_{rms}}$ as parameter ; values of $\frac{\overline{x_2 x'_2}}{E_{rms}}$ and $\frac{\overline{x_2^2}}{E_{rms}}$ are also indicated, as well as curves along which the conditions :

$$\overline{x_2^2} = \overline{x_1^2}$$

$$\overline{x_2 x'_2} = -\overline{x_1 x'_1} \qquad (8)$$

apply. The conditions (8) ensure that the beam sizes and absolute values of divergences at AP1 and AP2 are the same ; this is probably the best requirement one can put on a limiting system.

Using Fig. 3, the length L of the beam limiting section has been fixed to 675 mm. Fig. 4 gives the conditions the beam has to satisfy at AP1 for a proportional limitation in diameter and divergence. The system of apertures has been analysed for beam currents up to 300 mA.

4. CHOICE OF THE BUNCHING SYSTEM - COMPUTING METHODS

The most important part of LEBT, but also the most delicate to design is the one where the beam is bunched and matched to the six-dimensional linac acceptance. One has already reported on the methods by which a bunching system is computed[4), 5)] and on the choice of convenient bunching schemes[6)] ; nevertheless, for the sake of completeness, one will summarize here the essential points:

The system of bunchers groups particles in the longitudinal phase plane $(z_1 z')$ in such a way as to fill optimally an ellipse defined by :

$$E_z = k^2 E_{zrms} = 5\left[\overline{z^2}\ \overline{z'^2} - (\overline{zz'})^2\right]^{\frac{1}{2}} ;$$

This ellipse is the marginal longitudinal emittance. The factor $k^2 = 5$ in the formula arises because we are considering an equivalent bunched beam, represented by a uniformly filled ellipsoid in real three dimensional space, see Appendix 1.

The emittance formed by the bunching process has to be matched to the longitudinal (linearised) acceptance of the Linac. Instead of using the (z,z') phase plane, one usually works with phase extensions $\Delta\phi$ and energy spreads ΔW ; in this case, the longitudinal emittance is expressed as :

$$E_z = 5 \frac{\beta\lambda}{2\pi W_s} \sqrt{\overline{\Delta\phi^2}\ \overline{\Delta W^2} - (\overline{\Delta\phi\Delta W})^2},$$

where β is the relativistic factor, λ the RF wave length and W_s the particle energy before bunching. A useful numerical form of the above formula (valid for W_s = 750 keV) is :

$$E_z = 0.5555 \sqrt{\overline{\Delta\phi^2}\ \overline{\Delta W^2} - (\overline{\Delta\phi\Delta W})^2} \quad \text{(mm.mrad)},$$

with $\Delta\phi$ in degrees and ΔW in keV.

An efficient bunching can be obtained with two bunchers, the first working on the fundamental RF frequency and the second on its harmonic ; such a system is called a double drift harmonic buncher[7] (DDHB).

The longitudinal rms emittance, formed by the DDHB, depends on the number of particles which are contained in it (this number is, of course, not known a priori, but it is determined in the course of optimization by the program PREINJ)[3,4], on the bunching voltages V_{B1} and V_{B2}, and on the distance d_{12} between bunchers ; in total four parameters. The distance of the second buncher to the linac, d_{2L}, makes the fifth parameter. To match two ellipses (emittance and acceptance) one needs in principle only three parameters, so for the two remaining ones additional constraints can be imposed.

The energy modulation imparted to the beam by the DDHB is shown in Fig. 5. The form of this modulation (in the $\Delta\phi$, ΔW plane) is essential for the bunching efficiency and it has to be optimised as function of linac input conditions and beam intensities.

It has been found that the form of the modulation curve $W = f(\Delta\phi)$ depends only on the ratio of buncher voltages $\frac{V_{B2}}{V_{B1}}$ (the absolute value of the voltages is merely a proportionality factor for the extension of the curve in the ΔW direction) and on a parameter ψ_{12}. The latter has the dimension of an angle whose geometrical meaning and analytic expression are shown in Fig. 5b. One has the following equations :

$\Delta W_1 = - V_{B1} T_1 \sin \Delta\phi_1$ ... energy modulation of a particle with phase $\Delta\phi_1$ at first buncher

$\Delta\phi_2 = \Delta\phi_1 - \psi_{12} \sin \Delta\phi_1$ ... phase of the above particle at second buncher

$\Delta W = \Delta W_1 + V_{B2} T_2 \sin \Delta\phi_2 = \Delta W_1 + V_{B2} T_2 \sin (\Delta\phi_1 - \psi_{12} \sin \Delta\phi_1)$

... total energy modulation after second buncher

Normalized modulation :

$$\frac{\Delta W}{V_{B1} T_1} = \frac{\Delta W_1}{V_{B1} T_1} + v \sin (\Delta\phi_1 - \psi_{12} \sin \Delta\phi_1) ,$$

where v stands for the ratio $\frac{V_{B2} T_2}{V_{B1} T_1}$.

All the particles passing through the first buncher with a phase $\Delta\phi_1$ comprised between a certain $\Delta\phi_{1_{min}}$ and $\Delta\phi_{1_{max}}$ will be trapped ; they will form the longitudinal emittance, whose size will depend also on the modulation curve, which in turn depends on v and ψ_{12}. On can put $E_z = f(v, \psi_{12})$, where the number of particles between $\Delta\phi_{1_{min}}$ and $\Delta\phi_{1_{max}}$ enters as parameter (this parameter, η, is usually normalized, indicating automatically the trapping efficiency). For each η, one can find a combination of values v and ψ_{12} which minimize E_{zrms}, which in other words means maximising the bunching efficiency. Values of v and ψ_{12} obtained by an optimisation procedure are the additional constraints we have imposed on the bunching scheme.

The energy modulation process, as represented in Fig. 5, is only an approximation ; in fact the amount of modulation depends also on the radial position of particles and is given approximately by the radial variation of the transit time factor :

$$T \tilde{=} T_a \left(1 + \frac{k_r^2}{4} r^2\right) \tilde{=} T_a \left[1 + \frac{1}{4}\left(\frac{2\pi}{\beta\lambda}\right)^2 (x^2 + y^2)\right] ,$$

where T_a is the transit time factor on the axis and x and y are the transverse coordinates of the particle. For a more accurate treatment of bunching, the beam is divided into concentric elliptical rings, each containing the same number of particles, and a mean transit time factor $T_i \tilde{=} T_a \left[1 + \frac{k_r^2}{4} (x_i^2 + y_i^2)\right]$ is determined for each ring i. In Appendix 2 one has shown the calculations by which one determines the rings and the T_i's for different density distributions. In Fig. 6, modulation curves are presented for a beam divided into five rings ; these curves are obtained by a program BUNNL[3]. Another program, OPTNL[3] considers the radial extension of the beam at DDHB and its density distribution and searches for values of v and ψ_{12} resulting in a minimum E_{zrms}. Typical results are shown in Fig. 7.

Having introduced additional constraints for the bunching system, one is now left with three parameters, and as d_{2L} has to be fixed (e.g. to satisfy conditions for a "nominal" case), one can in reality vary only two of them. To obtain a matched beam for different operating conditions of the linac, one has either to drop a constraint or to modify the bunching system. In fact, it has been found that flexibility in operation over a wide current range and with a good bunching efficiency is obtained when introducing a third buncher, close to the linac. This additional buncher (which in previous reports we called "energy spread corrector"), operates on the fundamental RF frequency and improves particularly the situation when working with higher beam currents, as it compensates for the loss of energy modulation coming from the action of space charge forces. Hence, the bunching system for the LEBT is composed of three bunchers, the DDHB and the "energy spread corrector". It should be noted that the "energy spread corrector" changes the inclination of the longitudinal emittance, but does not affect its magnitude significantly, because the beam is already so bunched that it passes through the buncher during the ∿ linear portion of the sinusoidal modulation voltage (the energy spread corrector will hereafter be called the third buncher). The computer program PREINJ has been used to optimise the layout and to find the buncher and quadrupole settings for various beam intensities and linac operating conditions. The results are reported in chapter 6.

5. OPTIMISATION OF THE BUNCHING SCHEME

The design of the bunching system has so far been based on computational methods permitting the use of linear optimisation routines : in PREINJ the beam is represented as an entity and all the forces linearised. One needs therefore to check the results, in particular with respect to non-linear phenomena arising from non-uniform density distributions in the beam. Such phenomena can be revealed by the use of multi-particle programs; a program of this type, BUNCH 74[8], improved to suit our demands, has been used in combination with PREINJ and the design, where necessary, modified. The phenomena one has analysed are the following :

a) Transverse emittance growth due to non-linear space charge forces (in PREINJ only the emittance growth due to a longitudinal - transverse coupling in the bunchers is included, see Fig. 8).

b) Longitudinal emittance growth (with very narrow beams, the irregular local high densities give rise to emittance blow-up; the best trapping efficiency is obtained when the transverse beam size in bunchers is optimized as a compromise between transverse emittance blow-up (large beam) and longitudinal emittance (narrow beam)).

c) Filling of the longitudinal emittance with particles : in the course of the bunching optimisation with PREINJ, a longitudinal emittance is defined by particles lying in a certain phase range ; in spite of their contribution to the definition of E_z, some of these particles stay outside the ellipse, see Fig. 9a. It has been found by a combined use of PREINJ and BUNCH 74, that a slight modification of v and ψ_{12} can improve the trapping (one refers to the trapping efficiency indicated by BUNCH 74). A correction factor δ has therefore been introduced for these parameters, depending on the beam intensity and density distribution ; see Fig. 9b, where the bunching efficiency of LEBT is shown as function of δ. The efficiency calculated by PREINJ has, of course, a maximum for $\delta = 1$; on the contrary, BUNCH 74 shows maxima in the region $\delta = 0.85 \div 0.925$. These latter maxima are considered as the significant ones. It should be noted that the values in Fig. 9b apply for the narrowest beam one intends to inject into the linac[9] (strongest focusing in tank I : $\mu^{*)} \tilde{=} 39^0$) ; for wider beams, the bunching efficiency is higher, compare Fig. 24, but larger beams are less favourable for acceleration.

---

*) μ is the betatron phase advance per structure period ; the new linac will operate with an FD focusing.

d) Dependence of bunching efficiency on the density distribution in the beam : the matching optimisation in PREINJ depends on the rms values of the beam coordinates and is supposed to be valid for all ellipsoidal density distributions (apart from the "multi-ring" treatment of bunchers, see Appendix II) ; it is interesting therefore to check by BUNCH 74, how this basic assumption holds, in particular as the density distribution after bunching departs from an ellipsoidal one. Figs. 10 and 11 show results of BUNCH 74 for a uniform, parabolic and truncated Gaussian distribution (in real space*)) ; the bunching efficiencies are all within 77 ÷ 80% for a 200 mA preinjector beam.

e) Chances for a quick loss of non-trapped particles in the linac : one is interested to loose particles outside the longitudinal emittance ellipse as soon as possible. The third buncher, in fact, imparts to those particles big energy spreads and contributes to their elimination ; compare cases with and without third buncher, Figs. 11 and 12. (The beam intensity in Fig. 12 had to be reduced to 100 mA in order that the longitudinal space charge forces do not cancel the whole energy modulation).

Summing up, one can say that BUNCH 74 permitted us to introduce some refinements into our optimisation method, but it confirmed also the validity of the six-dimensional matching as obtained by PREINJ. It is even surprising that two so different methods, one dealing with linearised forces and treating the beam as an entity, the other considering particle by particle, yield results which differ by only a few percent.

6. DESIGN OF LEBT SECTIONS ; LAYOUT OF LEBT

Having analysed the methods underlying the design of LEBT, we shall now concentrate on the design itself. Two parts of LEBT have already been dealt with : the beam limiting and bunching sections. Before the limiting section, one has foreseen a section where the preaccelerator beam will be measured and matched to the first four-jaw aperture of the

---

*) If a n-dimensional hyperellipsoidal distribution in phase space has a certain form in real space, it has the same form also in velocity space.

limiting section. Before the bunchers, one has inserted a transition section, where the beam will be reduced in size, in order to meet the conditions at DDHB. Hence, the LEBT will be composed of four sections :

1. measuring section
2. limiting section
3. transition section
4. bunching section

} contain an empty drift space each

The measuring and transition sections contain two symmetric triplets each, sufficient to satisfy the matching requirements at the section output. The position of the triplets has been optimised by the linear program CTBEAM, taking into account imposed geometrical conditions. One has preferred triplets to doublets, because the former are more suited for producing round beams, a condition required for a minimum energy transfer between oscillations in the two transverse planes (condition for minimum emittance blow-up).

The limiting section will, in addition to four-jaw apertures, contain sieves of different transparency ; sieves reduce the beam intensity without affecting appreciably the emittance.

The design of the bunching section has followed the lines reported in chapters 4 and 5. As mentioned, the installation of the third buncher was intended to compensate for the space charge action, which reduced the energy spread imparted to the beam by the DDHB system. In the course of the design, one has investigated if a fuller use of the third buncher could be made by distributing the voltages on this buncher and DDHB in a different way ; one wanted essentially to lower the DDHB voltages and increase the voltage on the third buncher thus obtaining a reduction of the longitudinal emittance. (E_z is directly proportional to the voltages on DDHB ; the third buncher does not significantly increase E_z, as the beam is already sufficiently bunched to pass during the linear

portion of the bunching voltage). The bunching voltages change when changing the distance of DDHB to the linac ; several positions of DDHB have been analysed, but a rather flat efficiency curve has been found, see Fig. 13 (curve η_B). The distance of 81 cm has finally been chosen as a good compromise between efficiency, bunching voltages and geometrical considerations.

A schematic layout of LEBT, with the division into sections and with curves indicating beam envelopes and divergences is presented in Fig. 14. The curves apply to a nominal, equivalent beam (intensity 200 mA, uniform density distribution in real space). Fig. 15 details the matching conditions and gives the settings of quadrupoles and bunchers. A mechanical drawing of LEBT is shown in Fig. 16, with a list of apparatus to be installed in this region. A description of these apparatus is beyond the scope of this paper. It should be mentioned only that the electron traps are intended to prevent a partial beam neutralisation by electrons, which would be difficult to control ; the electron traps are, in addition, arranged in such a way as to be able to compensate for possible steering errors in LEBT.

7. OPERATION AT DIFFERENT BEAM INTENSITY LEVELS

The layout of LEBT has been optimised for the nominal preaccelerator beam current (200 mA) and for the most severe linac input conditions (beam diameter < 8 mm, corresponding to the strongest focusing foreseen for tank I : $\mu = 39^0$, with FD quadrupole connection). It is certainly interesting to analyse the behaviour of the LEBT for other beam intensities and matching conditions.

The matching conditions at the bunchers (DDHB) do not change significantly with beam intensity (the required beam diameter stays between 10 ÷ 12 mm), so the part of LEBT which handles the continuous (unbunched) beam has always the same output conditions to fulfill. One has tested this part of LEBT for intensities of up to 300 mA, see Fig. 17 ; a good transport and matching is possible (note that the conditions at the beam

limiting section change with beam intensity). In Figs. 18 and 19 one has represented beams which are not intended to be limited by the four-jaw aperture system : the matching conditions at AP1 are ignored and the beam is kept round and of roughly the same size until the last portion of the transition section.

The situation is different for the bunching section : its output conditions (i.e. the conditions at the linac input) change with beam intensity and with linac operating settings. If one does not vary the nominal accelerating field in tank I, the conditions at linac input are a function of I (intensity of trapped beam) and μ (betatron phase advance per structure period). These conditions are determined by a computer program dealing with beam dynamics in the linac, ADAPTEF[3] (an improved version of ADAPT[10]), and are represented in Figs. 20, 21 ; they apply to the end of the first half drift tube in tank I, which is considered as the linac input matching plane (the quadrupole in the first half drift tube is still a part of the LEBT matching scheme).

The bunching section has been tested for various beam intensities : Fig. 22 shows the transport of a 100 mA beam (a higher energy spread is required to match lower intensity beams, compare Fig. 20b), whilst Fig. 23 represents the situation with a 250 mA beam ; for the latter, one has maintained the same linac input conditions as for a 200 mA beam, which is a more severe requirement. In all the tests one has envisaged that the linac is operating with its highest μ value ($\sim 39^0$), a condition which brings about the highest space charge forces. The trapping efficiency stays always in the region of 77 ÷ 80%.

In Fig. 24 one has represented a case more relevant to a weaker focusing in the linac, $\mu = 15^0$; the matched transverse beam envelopes at linac input are larger ($\sim$ 6 mm), the space charge forces are lower and one obtains a bunching efficiency of 83% (with BUNCH 74). However, larger beams ungergo usually an emittance blow-up during acceleration in the linac.

8. OPERATION WITHOUT THE HARMONIC BUNCHER

Most of low energy beam transport systems working with bunchers do not contain harmonic bunchers and are in principle rather different from the system described in this paper. It is therefore interesting to analyse the operation of LEBT proposed for the new CERN linac with the harmonic buncher switched off ; the reasons for this analysis are two-fold :

a) Feasibility of operation of LEBT with bunchers of fundamental RF frequency only.

b) Comparison of results obtained by the two bunching schemes.

The program PREINJ has been used to optimise the settings of the bunching section with only the first and the third buncher in operation. It has been possible to obtain matching solutions, but, of course, with a smaller bunching efficiency. The results have been, as usual, checked by BUNCH 74 and an agreement found. In Figs. 25 and 26 one has represented a case for I = 250 mA, resulting in $\sim$ 140 mA accepted by the linac (according to BUNCH 74). It is instructive to compare these Figs. with Figs. 10 and 11 : the bunching with a DDHB system is superior to a single buncher not only from the point of view of efficiency ($\sim$ 78% compared to $\sim$ 55%), but also with respect to the way the longitudinal emittance is filled up.

9. CONCLUSION

In this paper one has tried to explain the approach which has led to the design of LEBT : the layout and the importance of various parameters have first been analysed by a whole series of linear programs, based on methods developed to solve beam optical problems and optimise the bunching. Thereafter, a multi-particle program, BUNCH 74, has been used to reveal non-linear phenomena and their significance, and to confirm eventually, the validity of principles on which the design has been based. A satisfactory agreement has finally been obtained between both types of programs.

In fact, even more computational tests have been made to check the performance of LEBT : D.J. Warner has modified the multi-particle program MAPRO 1[11] to be used in chain with the program BUNCH 74 and treat the acceleration of the LEBT beam in tank 1 of the new linac. An analysis of the beam dynamics in the linac tanks does not enter in the frame of this paper. However, one should mention that for the nominal operating conditions of the linac ($\mu = 39^0$), MAPRO 1 gives trapping efficiencies of $\sim$ 88% and $\sim$ 66% for the LEBT operating with and without the second harmonic buncher. (This high trapping efficiency is due to the dynamic increase of the stable area in the longitudinal phase plane : particles lying initially outside the bucket can in the course of acceleration be trapped).

This paper has dealt essentially with beam optics in the LEBT, and has shown that a good six-dimensional matching to the linac input can be obtained by the proposed design. Some problems have not been included, as beam steering, neutralisation by electrons, beam emittance and bunch measurements, etc. These problems should be treated in papers concerning apparatus installed in the LEBT area.

ACKNOWLEDGEMENT

The design of LEBT has profited from discussions in the linac design committee ; in particular, we would like to acknowledge the collaboration of D.J. Warner (beam optics) and E. Boltezar (mechanical layout), as well as the useful comments of P. Lapostolle (CNET, Paris) and M. Promé (CEN, Saclay), made during our meetings in the past year.

REFERENCES

1. F. Sacherer, RMS envelope equations with space charge, CERN/SI/Int.70-12.

2. D.J. Warner (editor), Project study for a new 50 MeV linear accelerator for the CPS, CERN/MPS/LINP 73-1.

3. B. Bru and M. Weiss, Linear optimisation programs dealing with beam optics in the linear accelerator complex, CERN/MPS/LIN 74-2.

4. B. Bru and M. Weiss, Computational methods and computer programs for linearised analysis of periodic structures and beam transport systems under space charge conditions, CERN/MPS/LIN 72-4.

5. M. Weiss, Bunching of intense proton beams with six-dimensional matching to the linac acceptance, Proc. of the 1973 Part. Acc. Conf., San Francisco, p. 877, and CERN/MPS/LIN 73-2.

6. B. Bru and M. Weiss, Single and double-drift bunchers as possible injection schemes for the CPS linac, Proc. of the 1973 Part. Acc. Conf., San Francisco, p. 963, and CERN/MPS/LIN 73-1.

7. C.R. Emigh, Double-drift buncher, Proc. 1968 Proton Linear Acc. Conf., Brookhaven.

8. B. Bru and D.J. Warner, Bunch 74, an improved multiparticle beam simulation program, CERN/MPS/LIN 74-3.

9. D.J. Warner, Private communication.

10. B. Bru, Calcul de la focalisation quadrupolaire d'un linac et de l'adaptation du faisceau en présence de charge d'espace, thèse université de Lyon, 1970.

11. M. Promé, Effets de la charge d'espace dans les accélérateurs linéaires à protons, thèse, université de Paris-Sud, 1971.

CERN/MPS/LIN 74-1
Appendix I

SOME USEFUL FORMULAE CONCERNING RMS VALUES OF VARIOUS DENSITY DISTRIBUTIONS

The beam occupies in a n-dimensional phase space a hyperellipsoid (n = 4 for a continuous beam, n = 6 for a bunched beam) ; for simplicity of calculations, such a hyperellipsoid is usually transformed into a hypersphere. The density distributions one is dealing with are of the ellipsoidal type, i.e. they are represented in a hypersphere by a function f(r), where r is the radial variable in n dimensions :

$$r^2 = \sum_i^n x_i^2$$

The rms values of a density distribution are significant for the adjustment of matching parameters ; the knowledge of the ratio of rms values to marginal ones is important for the determination of apertures in a beam transport system.

The volume of a hypersphere is :

$$V = \int_0^{\hat{r}} \Omega_n r^{n-1}\, dr = \Omega_n \int_0^{\hat{r}} r^{n-1}\, dr$$

where n is the number of dimensions, Ω_n the corresponding space angle (equivalent to the surface area of a unit hypersphere) and $\hat{r}$ the radius. The rms value of any coordinate of the hypersphere is calculated as :

$$\tilde{x}_i = \left(\frac{1}{n} r^2\right)^{\frac{1}{2}} = \left(\frac{1}{n} \frac{\int_0^{\hat{r}} r^2 f(r) \Omega_n r^{n-1}\, dr}{\int_0^{\hat{r}} f(r)\, \Omega_n\, r^{n-1}\, dr} \right)^{\frac{1}{2}} = \left(\frac{1}{n} \frac{\int_0^{\hat{r}} f(r) r^{n+1} dr}{\int_0^{\hat{r}} f(r)\, r^{n-1} dr} \right)^{\frac{1}{2}}$$

We shall analyse the following distributions :

a) Kapchinsky - Vladimirsky

b) uniform

c) parabolic

d) Gaussian

I.1. Kapchinsky - Vladimirsky distribution

This is a surface distribution given by the δ function. The rms value is calculated by applying the above formula :

$$\tilde{x}_i = \left(\frac{1}{n} \frac{\int_0^{\hat{r}} \delta(r - \hat{r})\, r^{n+1}\, dr}{\int_0^{\hat{r}} \delta(r - \hat{r})\, r^{n-1}\, dr} \right)^{\frac{1}{2}} = \frac{\hat{r}}{\sqrt{n}} \; ;$$

The ratio of the rms value to the marginal one is :

$$\boxed{\frac{\tilde{x}}{\hat{x}} = \frac{1}{\sqrt{n}}} \qquad (\text{note } \hat{x} = \hat{r}) \qquad (1)$$

I.2. Uniform distribution

Proceeding in the same way as above, one has :

$$\tilde{x}_i = \left(\frac{1}{n} \frac{\int_0^{\hat{r}} r^{n+1}\, dr}{\int_0^{\hat{r}} r^{n-1}\, dr} \right)^{\frac{1}{2}} = \frac{\hat{r}}{\sqrt{n+2}} \quad , \text{ or}$$

$$\boxed{\frac{\tilde{x}_i}{\hat{x}} = \frac{1}{\sqrt{n+2}}} \qquad (2)$$

Example : $\dfrac{\tilde{x}_i}{\hat{x}} = \frac{1}{2}$ for n = 2

The same result is obtained with a Kapchinsky-Vladimirsky distribution for n = 4.

I.3. Parabolic distribution

$$\tilde{x}_i = \left(\frac{1}{n} \frac{\int_0^{\hat{r}} \left[1 - \left(\frac{r}{\hat{r}} \right)^2 \right] r^{n+1} \, dr}{\int_0^{\hat{r}} \left[1 - \left(\frac{r}{\hat{r}} \right)^2 \right] r^{n-1} \, dr} \right)^{\frac{1}{2}} = \frac{\hat{r}}{\sqrt{n+4}} \qquad (3)$$

$$\boxed{\frac{\tilde{x}}{\hat{x}} = \frac{1}{\sqrt{n+4}}}$$

One can easily see that the results of a parabolic distribution for n = 2 correspond to those of a uniform distribution for n = 4.

I.4. Gaussian distribution

A n-dimensional Gaussian distribution is given by :

$$\prod_{}^{n} e^{-\frac{x_i^2}{2\sigma_i^2}}$$

and it extends, by definition, to infinity. The rms value of a coordinate is $\tilde{x}_i = \sigma_i$, as is well known.

If a Gaussian distribution is used to describe a beam, it has to be truncated at finite values of x_i ; in such a case $\tilde{x}_i \neq \sigma_i$ and the rms value is calculated as follows :

$$\tilde{x}_i = \left(\frac{1}{n} \frac{\int_0^{\hat{r}} e^{-\frac{r^2}{2\sigma^2}} r^{n+1} dr}{\int_0^{\hat{r}} e^{-\frac{r^2}{2\sigma^2}} r^{n-1} dr} \right)^{\frac{1}{2}} = \frac{\hat{r}}{\sqrt{n}} \left(\frac{\int_0^{1} e^{-\frac{r^2}{2\sigma_0^2}} r^{n+1} dr}{\int_0^{1} e^{-\frac{r^2}{2\sigma_0^2}} r^{n-1} dr} \right)^{\frac{1}{2}}$$

with $\sigma_0 = \frac{\sigma}{\hat{r}}$. One recognizes that the nominator in the above expression in brackets is in fact the negative derivative of the denominator with respect to the parameter $\frac{1}{2\sigma_0}$; putting $\frac{1}{2\sigma_0} = \alpha$ and writing the denominator as $I(\alpha)$ one has :

$$\frac{\tilde{x}_i}{\hat{x}} = -\frac{1}{\sqrt{n}} \left(\frac{I'(\alpha)}{I(\alpha)} \right)^{\frac{1}{2}} \text{ , where } I'(\alpha) = \frac{dI(\alpha)}{d\alpha} \quad .$$

The integral $I(\alpha)$ is solved by recurrence and it leads either to the Gaussian error integral (for n odd) or to an elementary integral (for n even). We shall analyse the latter case for n = 4.

Integrating the denominator one obtains :

$$I(\alpha) = \frac{1}{2\alpha^2} \left[1 - e^{-\alpha}(1 + \alpha) \right]$$

The derivation :

$$I'(\alpha) = \frac{1}{2\alpha^3} \left[\alpha^2 e^{-\alpha} - 2 + 2e^{-\alpha}(1 + \alpha) \right]$$

The ratio of rms to marginal value becomes :

$$\frac{\tilde{x}_i}{\hat{x}} = -\frac{1}{2} \left(\frac{\alpha^2 e^{-\alpha} - 2 + 2e^{-\alpha}(1 + \alpha)}{\alpha - \alpha e^{-\alpha}(1 + \alpha)} \right)^{\frac{1}{2}}$$

Simplifying and introducing again σ_0, one obtains :

$$\frac{\tilde{x}}{\hat{x}} = \left(\sigma_0^2 - \frac{e^{-\frac{1}{2\sigma_0^2}}}{8\sigma_0^2 \left[1 - e^{-\frac{1}{2\sigma_0^2}} \left(1 + \frac{1}{2\sigma_0^2} \right) \right]} \right)^{\frac{1}{2}} \qquad (4)$$

This is the ratio of rms to marginal value of a truncated Gaussian distribution for n = 4 ; in Fig. 1 one has represented $\frac{x}{\hat{x}}$ as function of σ_0.

I.5. Ratio between rms and marginal emittance

The rms emittance in a phase plane (x,x') is defined with :

$$E_{rms} = \left[\overline{x^2}\ \overline{x'^2} - (\overline{xx'})^2 \right]^{\frac{1}{2}}$$

If the ratio of the marginal value of a coordinate to the rms one is k, then the corresponding ratio of emittances is :

$$\frac{E}{E_{rms}} = k^2$$

Examples :

a) uniform distribution, n = 2 → k = 2 and $\frac{E}{E_{rms}} = 4$
(applies for uniform, continuous beams)

b) uniform distribution, n = 3 → k = $\sqrt{5}$ and $\frac{E}{E_{rms}} = 5$
(applies for uniform, bunched beams)

"MULTI-RING" METHOD APPLIED TO OPTIMISE THE BUNCHING EFFICIENCY

The acceleration of a particle in a RF gap depends on the radial position of the particle and is described by the modified Bessel function of zero order, contained in the expression for the transit time factor. An approximate formula is :

$$T \tilde{=} T_a \left(1 + \frac{k_r^2}{4} r^2\right) ,$$

the meaning of symbols being the usual one.

When optimising the bunching, in particular when dealing with the DDHB system, one has to take the variation of T across the beam cross-section into account. The best thing to do is to divide the beam in n-rings (an unbunched beam is represented by a cylinder), each one containing the same number of particles, and then define for each ring a mean transit time factor T_i :

$$T_i \tilde{=} T_a \left(1 + \frac{k_r^2}{4} \overline{r_i^2}\right)$$

The bunching optimisation is done by taking into account that the bunching in each ring is different.

The division into "equal current" rings depends on the density distribution. We shall analyse continuous beam having transversely a uniform, parabolic or Gaussian density distribution.

II.1. Uniform distribution

Dividing the beam into n-rings, each ring will contain $\frac{1}{n}$th of the total current ; for ring i (between radii r_{i-1} and r_i) one has :

$$\int_{r_{i-1}}^{r_i} rdr = \frac{1}{n}\int_{o}^{\hat{r}} rdr, \text{ or}$$

$$r_i^2 - r_{i-}^2 = \frac{\hat{r}^2}{n} \text{ , or } \underline{r_i^2 = r_{i-1}^2 + \frac{\hat{r}^2}{n}}$$

For i = 1 : $r_1^2 = \frac{\hat{r}^2}{n}$

For i = 2 : $r_2^2 = r_1^2 + \frac{\hat{r}^2}{n} = \frac{2}{n}\hat{r}^2$

In general for the radius r_i one has the formula :

$$r_i^2 = \frac{i}{n}\hat{r}^2 \qquad (1)$$

The formula for the mean transit time factor in ring i contains the quadratic mean value of the radius in that ring :

$$\overline{r_i^2} = \frac{\int_{r_{i-1}}^{r_i} r^3\, dr}{\int_{r_{i-1}}^{r_i} rdr} = \frac{1}{2}\frac{r_i^4 - r_{i-1}^4}{r_i^2 - r_{i-1}^2} = \frac{r_i^2 + r_{i-1}^2}{2}$$

Using formula (1) one gets :

$$\boxed{\overline{r_i^2} = \frac{2i - 1}{n} \hat{r}^2} \qquad (2)$$

II.2. Parabolic distribution

Proceeding as in II.1., one has :

$$\int_{r_{i-1}}^{r_i} \left[1 - (\frac{r}{\hat{r}})^2\right] r dr = \frac{1}{n} \int_{o}^{\hat{r}} \left[1 - (\frac{r}{\hat{r}})^2\right] r dr \; ;$$

integrated and rearranged :

$$\underbrace{\frac{r_i^2}{2} - \frac{r_i^4}{4\hat{r}^2}}_{f_i} = \underbrace{\frac{r_{i-1}^2}{2} - \frac{r_{i-1}^4}{4\hat{r}^2}}_{f_{i-1}} + \underbrace{\frac{1}{n} \frac{\hat{r}^2}{4}}_{K}$$

$$f_i = f_{i-1} + K$$

This is a recurrence formula, where f_i is expressed by f_{i-1} and a constant term K.

For i = 1 : $f_1 = K$

For i = 2 : $f_2 = f_1 + K = 2K$

In general: $f_i = iK$, or

$$\frac{r_i^2}{2} - \frac{r_i^4}{4\hat{r}2} = \frac{i}{n} \frac{\hat{r}^2}{4}$$

$$r_i^4 - 2\hat{r}^2 r_i^2 + \frac{i}{n} \hat{r}^4 = 0$$

For the radius r_i one gets finally :

$$\boxed{r_i^2 = \hat{r}^2 \left(1 - \sqrt{1 - \frac{i}{n}}\right)} \qquad (3)$$

The quadratic mean radius in ring i is defined as :

$$r_i^2 = \frac{\int_{r_{i-1}}^{r_i} \left[1 - \left(\frac{r}{\hat{r}}\right)^2\right] r^3 dr}{\int_{r_{i-1}}^{r_i} \left[1 - \left(\frac{r}{\hat{r}}\right)^2\right] r dr} ,$$

which after some calculations and using formula (3) gives :

$$\boxed{r_i^2 = \hat{r}^2 \left\{1 - \frac{2}{3}\left[\sqrt{\frac{n - i + 1}{n}}\,(n - i + 1) - \sqrt{\frac{n - i}{n}}\,(n - i)\right]\right\}} \qquad (4)$$

II.3. Gaussian distribution

Before analysing this distribution, a few remarks are necessary :

Unbunched beams are described either in the four-dimensional phase space or with projections in the two-dimensional real space. If the four-dimensional distribution is a Kapchinsky-Vladimirsky or a uniform one, the distribution of the two-dimensional projection is a uniform or a parabolic one. Only Gaussian distributions and their projections remain such for any number of dimensions ; this statement does not apply however for truncated Gaussian distributions, which are usually used in beam optical problems.

We shall analyse two- and four-dimensional truncated Gaussian distributions :

a) Gaussian distribution truncated in two dimensions :

$$\int_{r_{i-1}}^{r_i} e^{-\frac{r^2}{2\sigma^2}} r dr = \frac{1}{n} \int_{o}^{\hat{r}} e^{-\frac{r^2}{2\sigma^2}} r dr$$

$$\left[-\sigma^2 e^{-\frac{r^2}{2\sigma^2}} \right]_{r_{i-1}}^{r_i} = \left[-\frac{\sigma^2}{n} e^{-\frac{r^2}{2\sigma^2}} \right]_{o}^{\hat{r}} \text{ ; rearranged :}$$

$$\underbrace{e^{-\frac{r_i^2}{2\sigma^2}}}_{f_i} = \underbrace{e^{-\frac{r_{i-1}^2}{2\sigma^2}}}_{f_{i-1}} - \underbrace{\frac{1}{n}\left(1 - e^{-\frac{\hat{r}^2}{2\sigma^2}}\right)}_{K}$$

$i = 1 : f_1 = 1 - K$

$i = 2 : f_2 = f_1 - K = 1 - 2K$

In general :

$$f_i = 1 - iK \text{ , or}$$

$$e^{-\frac{r_i^2}{2\sigma^2}} = 1 - \frac{i}{n}\left(1 - e^{-\frac{\hat{r}^2}{2\sigma^2}}\right); \quad r_i \text{ can be expressed explicitly :}$$

$$\boxed{r_i = \left\{ -2\sigma^2 \ln \left[1 - \frac{i}{n}\left(1 - e^{-\frac{\hat{r}^2}{2\sigma^2}}\right)\right]\right\}^{\frac{1}{2}}} \qquad (5)$$

The quadratic mean of r in ring i is :

$$\overline{r_i^2} = \frac{\int_{r_{i-1}}^{r_i} e^{-\frac{r^2}{2\sigma^2}} r^3\,dr}{\int_{r_{i-1}}^{r_i} e^{-\frac{r^2}{2\sigma^2}} r\,dr} = \frac{\int_{r_{i-1}}^{r_i} e^{-\alpha r^2} r^3 dr}{\int_{r_{i-1}}^{r_i} e^{-\alpha r^2} r\,dr} = \frac{-\frac{\partial}{\partial\alpha}\int_{r_{i-1}}^{r_i} e^{-\alpha r^2} r\,dr}{\int_{r_{i-1}}^{r_i} e^{-\alpha r^2} r\,dr}$$

(see Appendix I.4.). After some calculations one gets :

$$\overline{r_i^2} = \left[2\sigma^2 + r_{i-1}^2 \frac{1 - \frac{i-1}{n}\left(1 - e^{-\frac{\hat{r}^2}{2\sigma^2}}\right)}{\frac{1}{n}\left(1 - e^{-\frac{\hat{r}^2}{2\sigma^2}}\right)} - r_i^2 \frac{1 - \frac{i}{n}\left(1 - e^{-\frac{\hat{r}^2}{2\sigma^2}}\right)}{\frac{1}{n}\left(1 - e^{-\frac{\hat{r}^2}{2\sigma^2}}\right)} \right]^{\frac{1}{2}} \qquad (6)$$

b) Gaussian distribution truncated in four dimensions :

For a Gaussian truncated in four dimensions, the two dimensional density distribution is expressed by[4] :

$$f(r) = \pi \int_{r^2}^{\hat{r}^2} f(R)\, d(R^2), \quad \text{with}$$

$$R^2 = x^2 + y^2 + x'^2 + y'^2 \quad ; \quad r^2 = x^2 + y^2 \quad \text{and}$$

$$f(R) = \text{const.}\ e^{-\frac{R^2}{2\sigma^2}}$$

Integrating one obtains :

$$f(r) = \text{const.} \left(e^{-\frac{r^2}{2\sigma^2}} - e^{-\frac{\hat{r}^2}{2\sigma^2}} \right)$$

Proceeding as under a) :

$$\int_{r_{i-1}}^{r_i} \left(e^{-\frac{r^2}{2\sigma^2}} - e^{-\frac{\hat{r}^2}{2\sigma^2}} \right) r dr = \frac{1}{n} \int_{o}^{\hat{r}} \left(e^{-\frac{r^2}{2\sigma^2}} - e^{-\frac{\hat{r}^2}{2\sigma^2}} \right) r dr$$

After some calculations :

$$\underbrace{e^{-\frac{r_{i-1}^2}{2\sigma^2}} + \frac{e^{-\frac{\hat{r}^2}{2\sigma^2}}}{2\sigma^2} r_{i-1}^2}_{f_{i-1}} - \left(\underbrace{e^{-\frac{r_i^2}{2\sigma^2}} + \frac{e^{-\frac{\hat{r}^2}{2\sigma^2}}}{2\sigma^2} r_i^2}_{f_i} \right) = \frac{1}{n} \left(\underbrace{1 - e^{-\frac{\hat{r}^2}{2\sigma^2}} - \frac{e^{-\frac{\hat{r}^2}{2\sigma^2}}}{2\sigma^2}}_{K} \right)$$

$$f_i = f_{i-1} - K$$

$i = 1 : \quad f_1 = 1 - K$

$i = 2 : \quad f_2 = f_1 - K = 1 - 2K$

In general : $f_i = 1 - iK$, or

$$\boxed{e^{-\frac{r_i^2}{2\sigma^2}} + \frac{e^{-\frac{\hat{r}^2}{2\sigma^2}}}{2\sigma^2} r_i^2 = 1 - \frac{i}{n} \left(1 - e^{-\frac{\hat{r}^2}{2\sigma^2}} - \frac{e^{-\frac{\hat{r}^2}{2\sigma^2}}}{2\sigma^2} \right)} \qquad (7)$$

From this expression one cannot derive an explicit formula for r_i. Therefore r_i as well as $\overline{r_i^2}$ has to be obtained numerically by computer programs.

Fig. 1: Ratio of rms to marginal value of a 4-dimensional gaussian distribution, truncated at $\hat{x}$

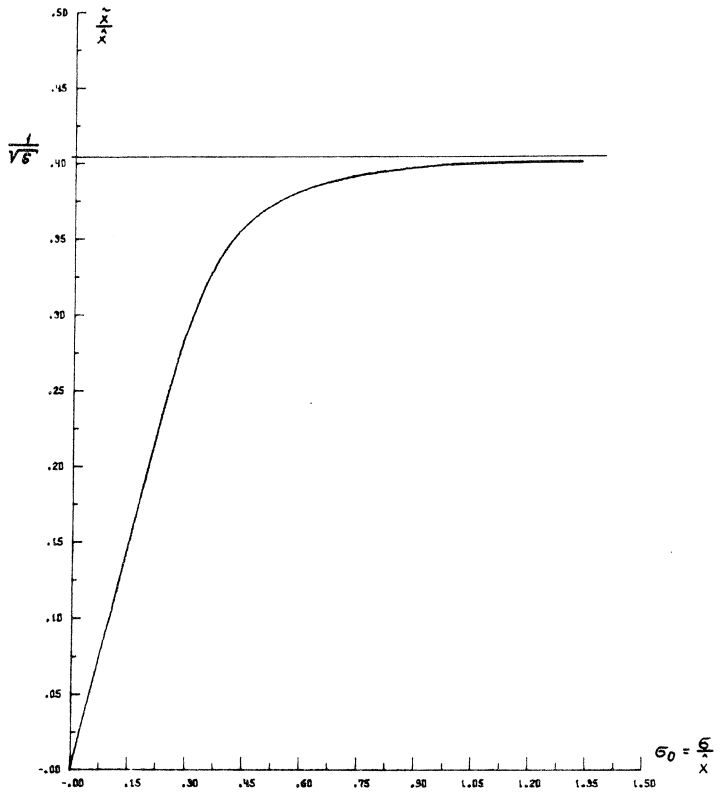

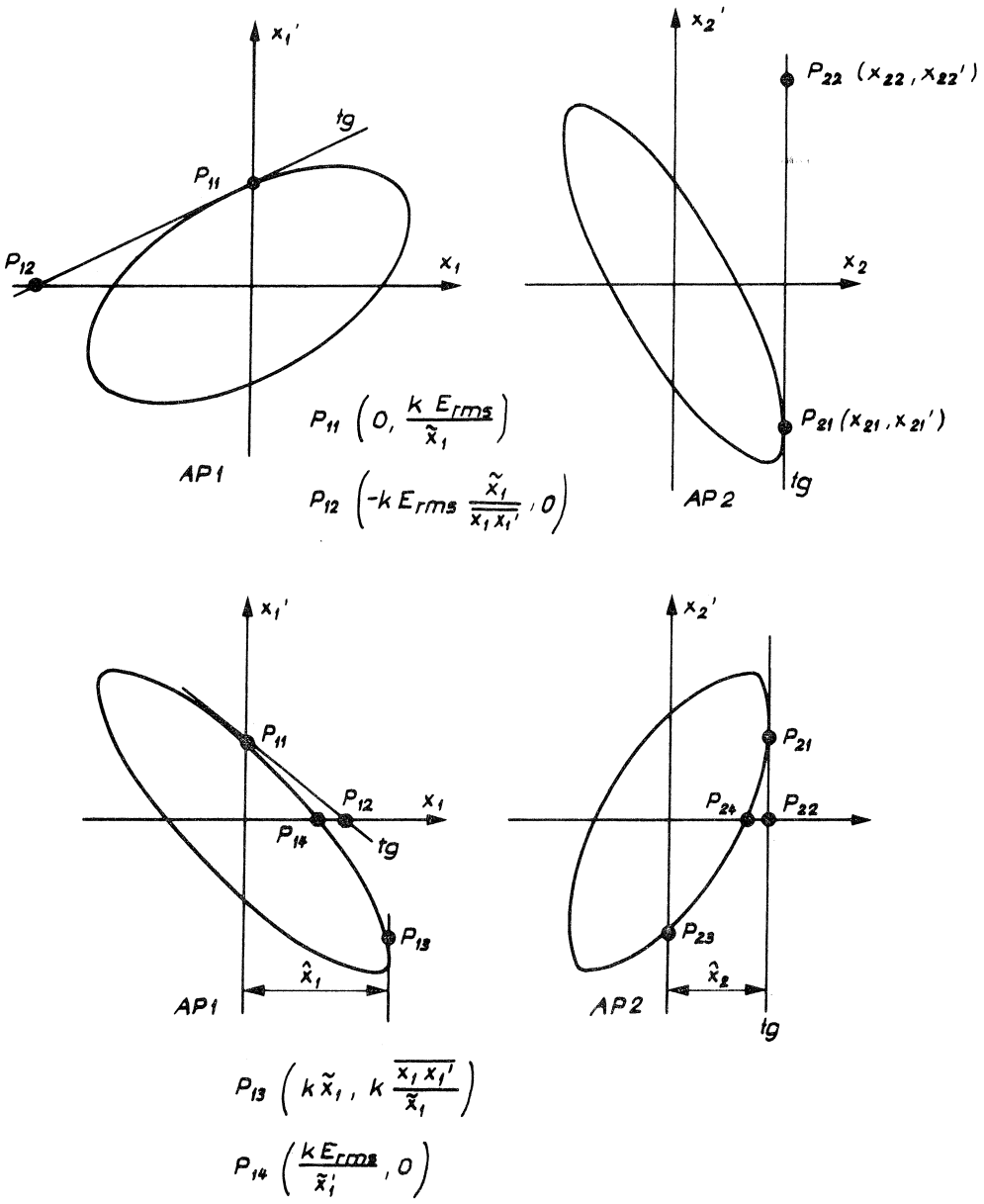

Fig. 2: Beam emittances at AP1 and AP2 for a proportional limitation in diameter and divergence

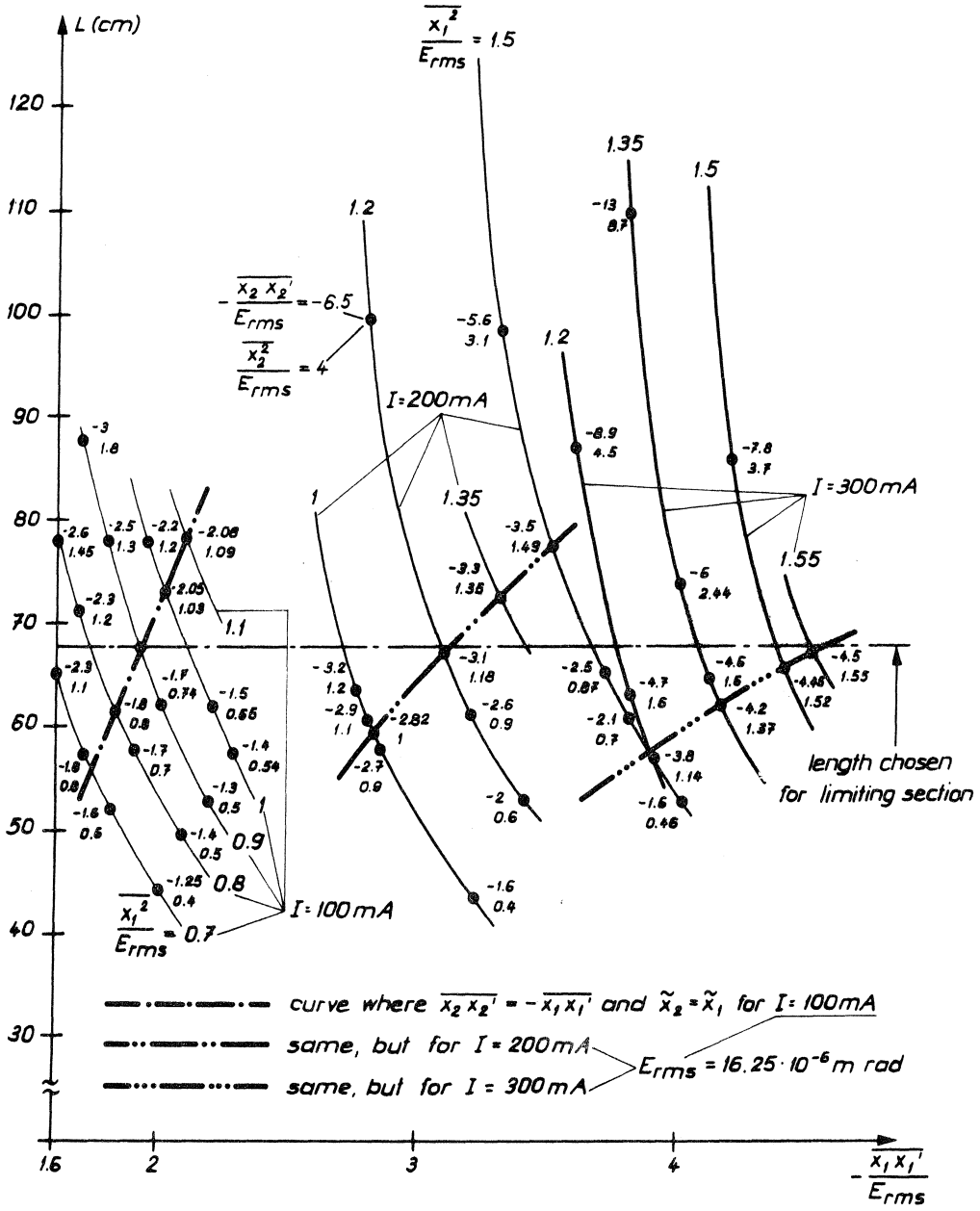

Fig. 3: Length of limiting section as function of input beam characteristics $\left(-\frac{\overline{x_1 x_1'}}{E_{rms}}, \frac{\overline{x_1^2}}{E_{rms}}, I\right)$ output values $\left(-\frac{\overline{x_2 x_2'}}{E_{rms}}, \frac{\overline{x_2^2}}{E_{rms}}\right)$ are indicated.

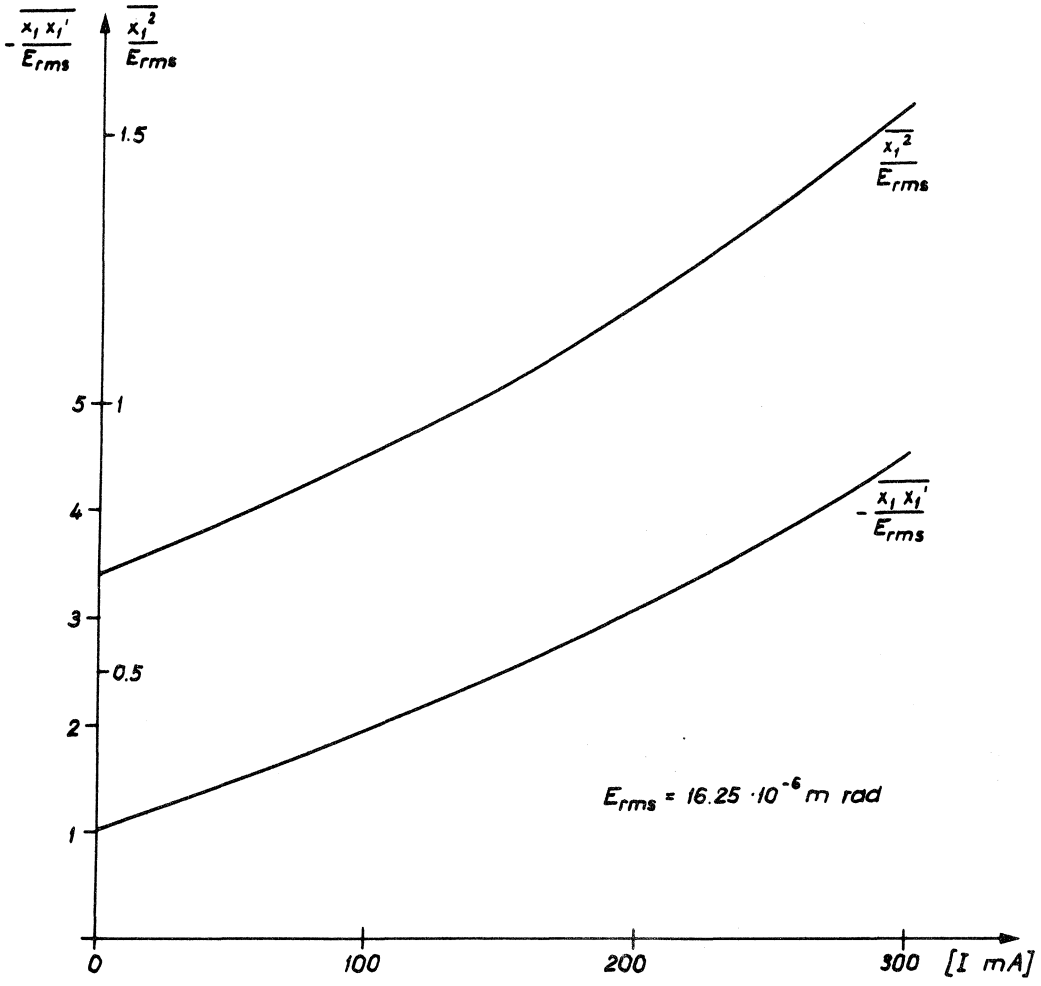

Fig. 4: Conditions at AP1 for a proportional beam limitation, satisfying the additional requirements $\tilde{x}_2 = \tilde{x}_1$ *and* $\overline{x_2 x_2'} = -\overline{x_1 x_1'}$

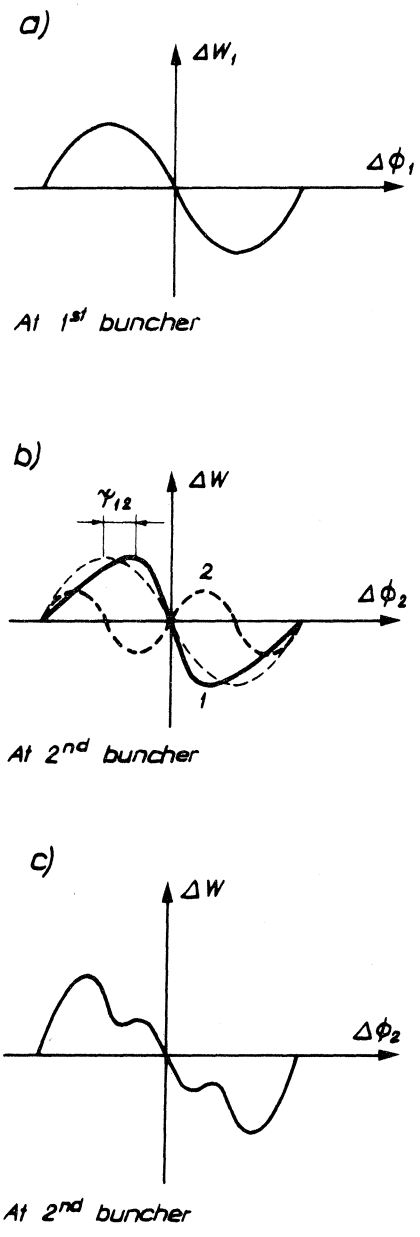

Modulation curve of 1st buncher:
$\Delta W_1 = -eV_{B1} T_1 \sin \Delta\phi_1$

1: transformed modulation curve of the 1st buncher:
$\Delta\phi_2 = \Delta\phi_1 - \psi_{12} \sin \Delta\phi_1$
with
$$\psi_{12} = \frac{\pi}{\beta\lambda} \frac{eV_{B1} T_1}{W_s} d_{12}$$

2: Modulation curve of 2nd buncher

Modulation curve of the DDHB system

Fig. 5: Energy modulation with DDHB

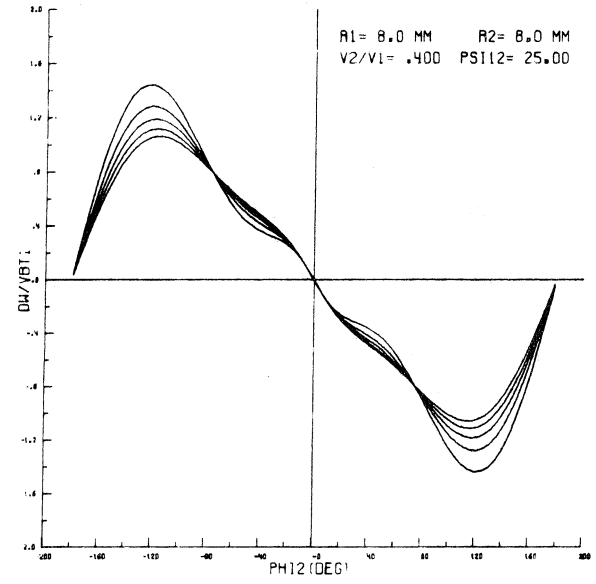

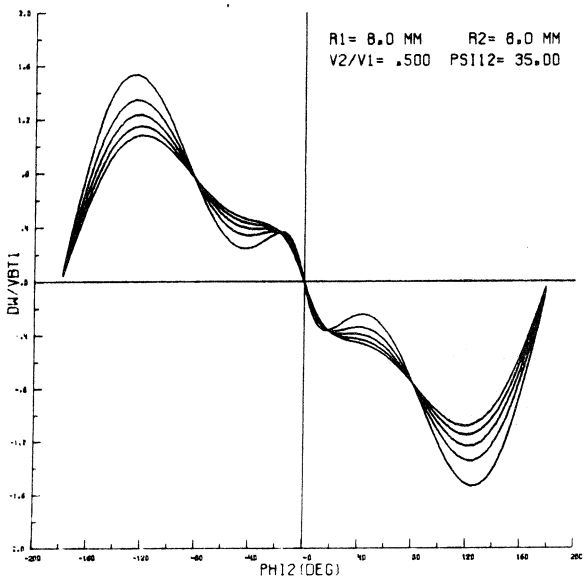

Fig. 6: Typical modulation curves of the DDHB system.

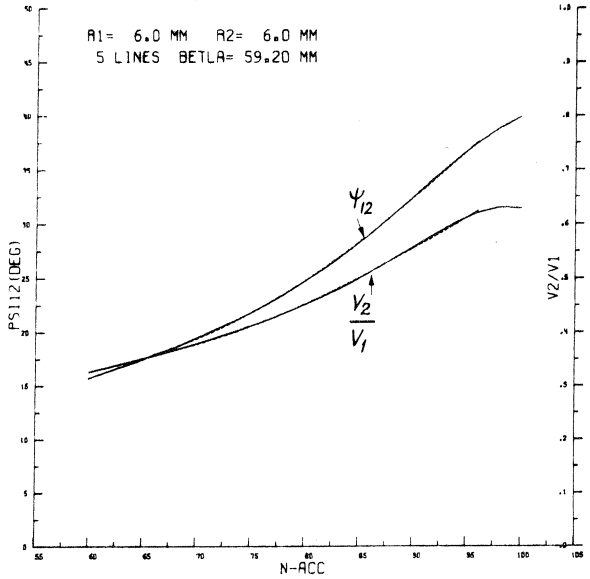

Fig. 7a: Values of $V_{B2}\ T_{2a} / V_{B1}\ T_{1a}$ and Ψ_{12} giving the minimum longitudinal emittance as function of the number of trapped particles; beam sizes at bunchers are parameters.

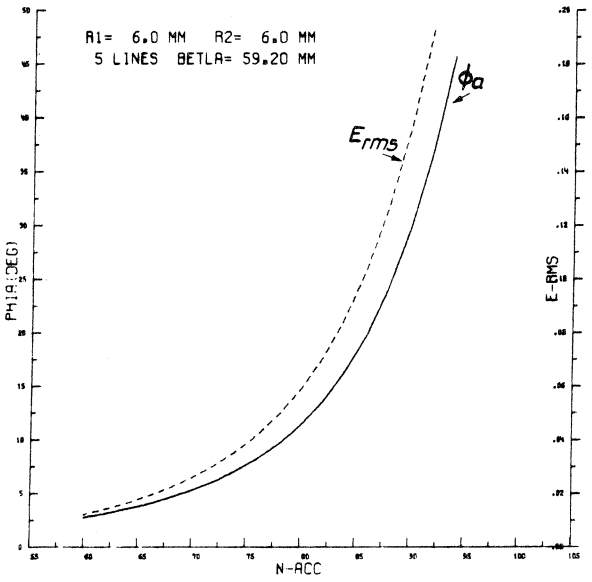

Fig. 7b: Minimum longitudinal rms emittance (normalized with $V_{B1}\ T_{1a} = 1$) and its half-width ϕ_a on the $\Delta\phi$ axis.

Fig. 8 : Relative increase of the transverse beam emittance in a buncher as function of bunching parameters and beam dimensions.

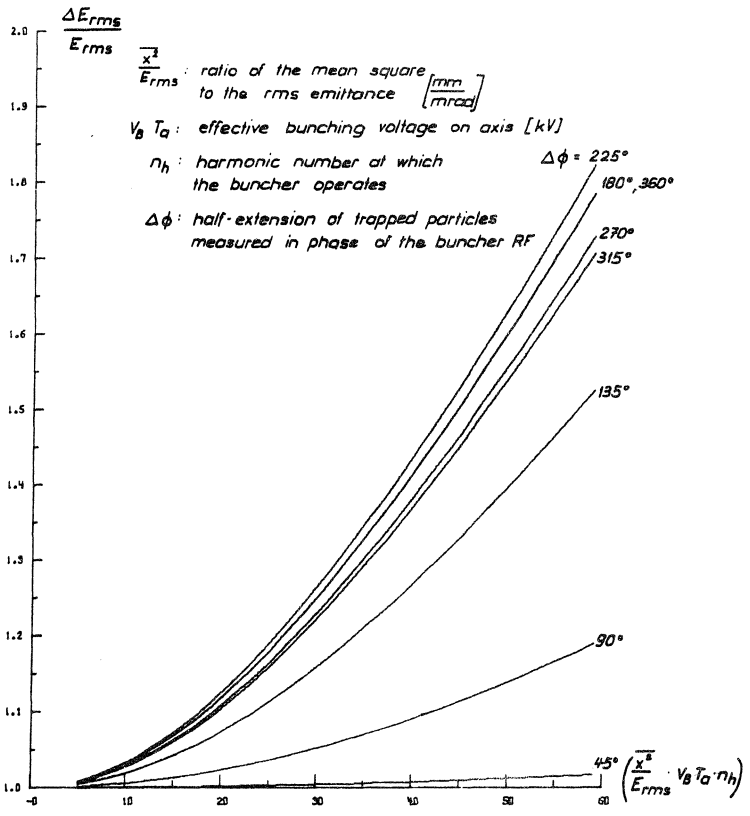

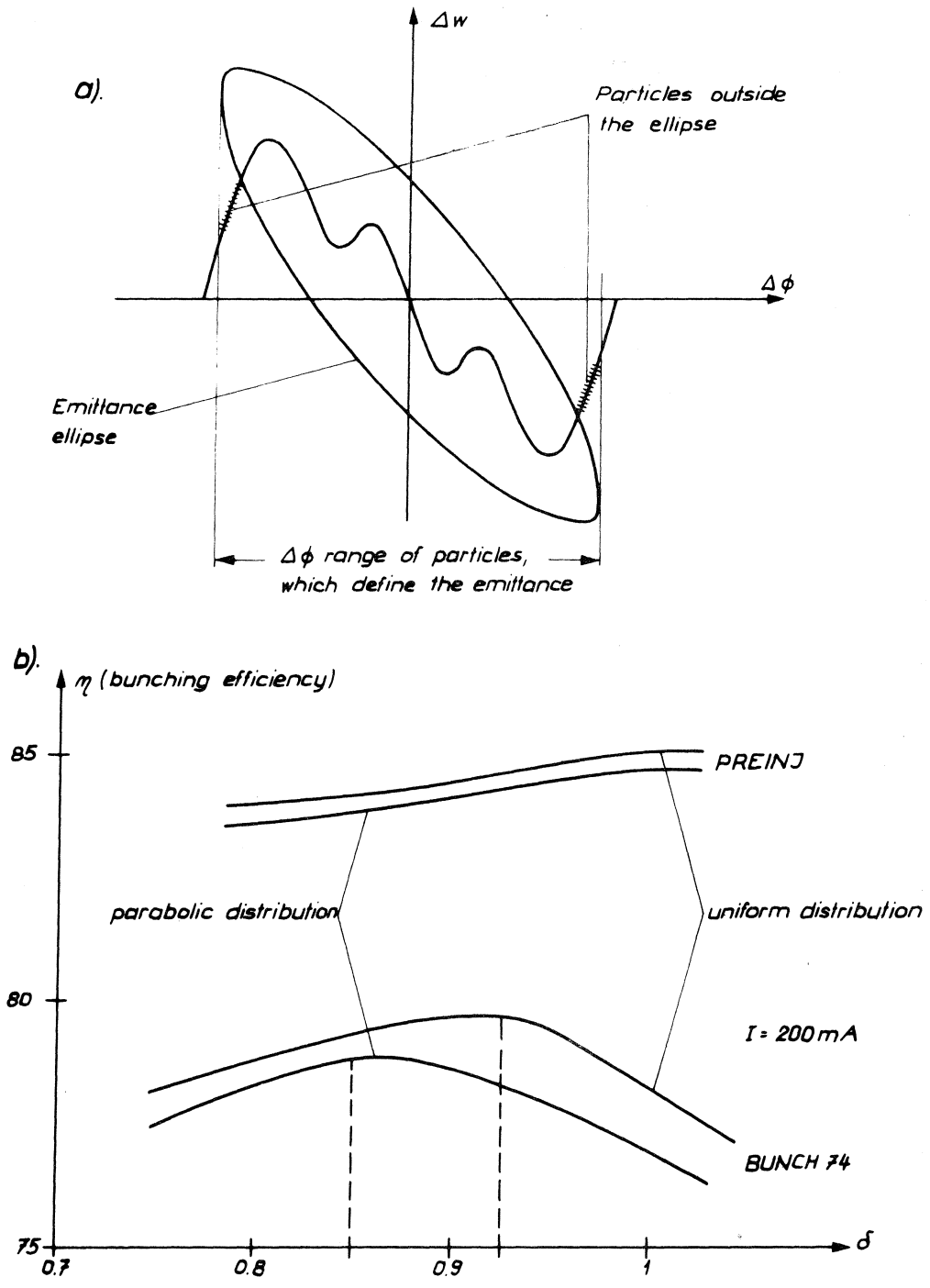

Fig. 9: Optimisation of bunching efficiency by introduction of a correction factor δ for V_{B2}/V_{B1} and φ_{12}

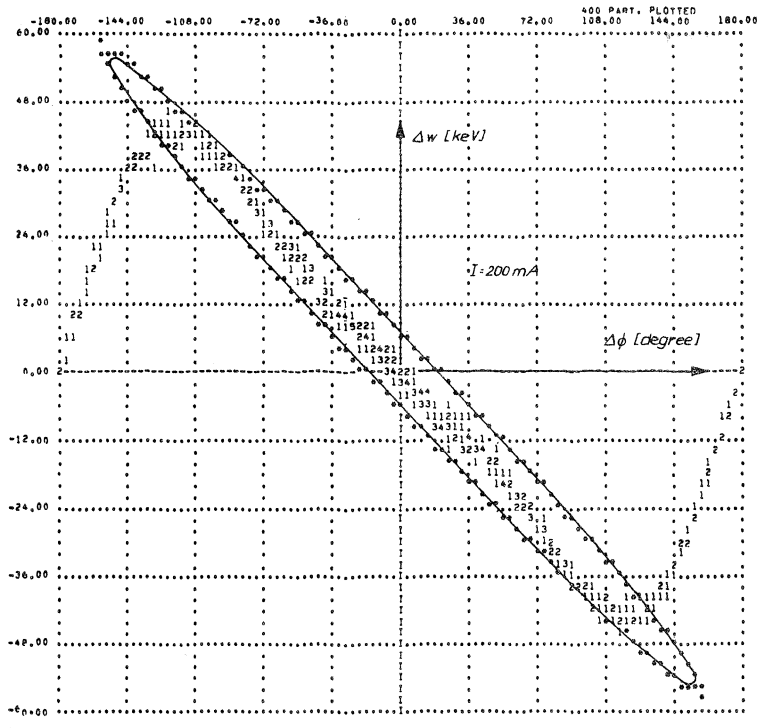

Fig. 10a: Scatter diagram in $(\Delta\phi, \Delta w)$ phase plane and the longitudinal beam emittance at 2nd buncher Uniform transverse density distribution in unbunched beam.

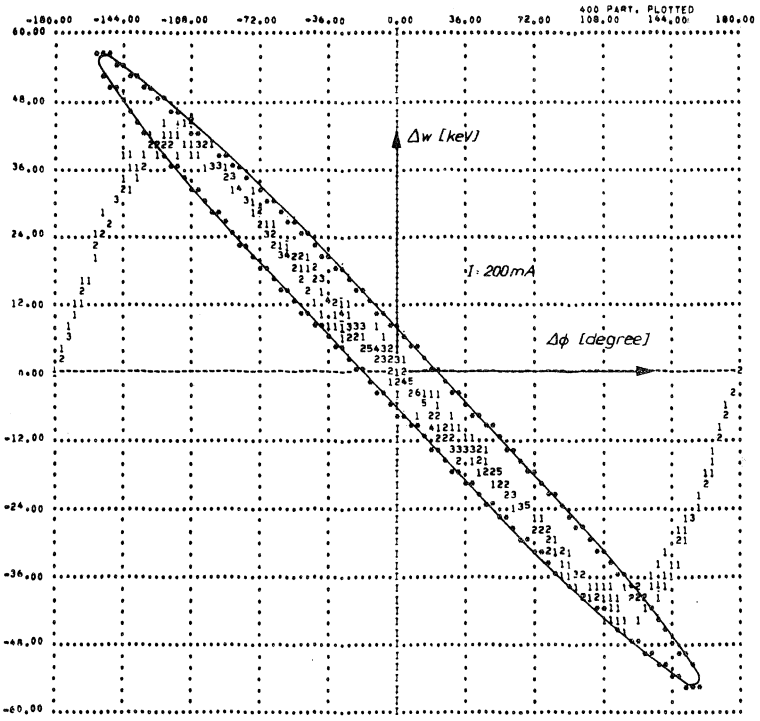

Fig. 10b: Same as 10 a, but with a parabolic density distribution.

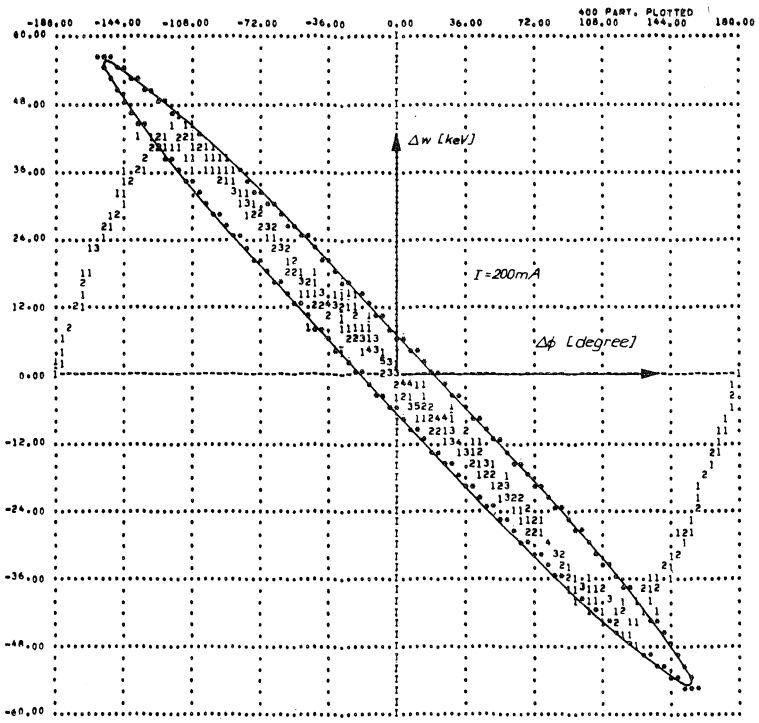

Fig. 10c: Same as 10a, but with a truncated gaussian density distribution.

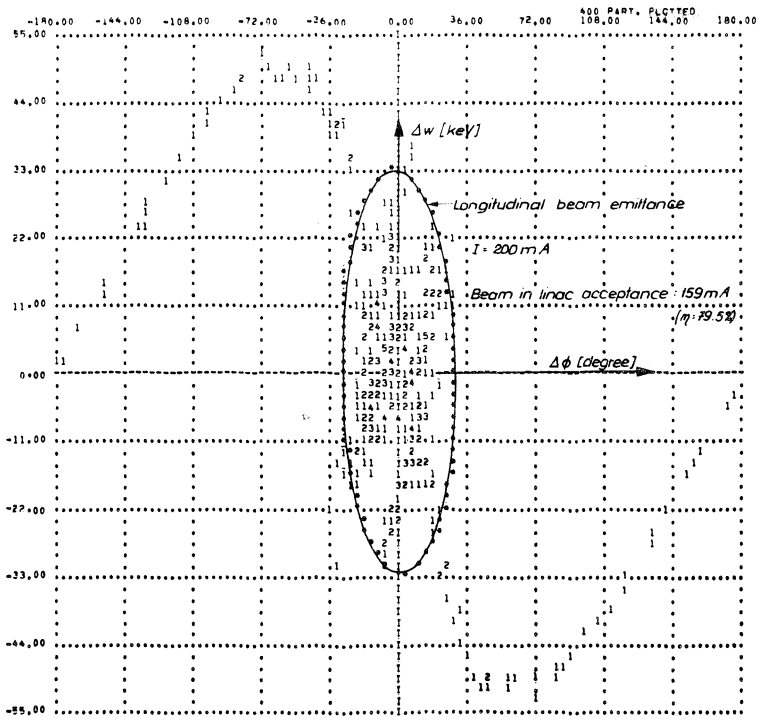

Fig. 11a: Scatter diagram in $(\Delta\phi, \Delta w)$ phase plane and the longitudinal beam emittance at linac input Uniform transverse density distribution in unbunched beam.

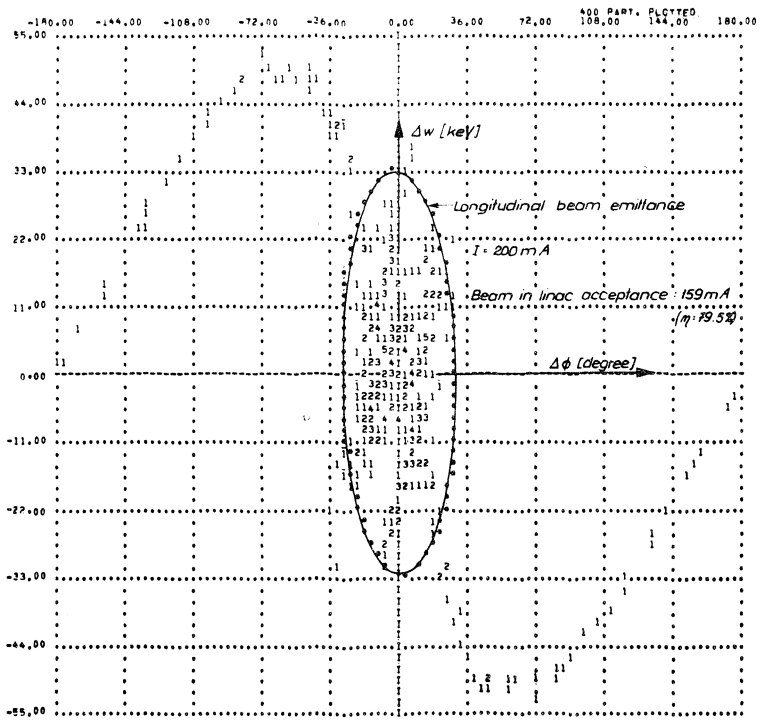

Fig. 11a: Scatter diagram in $(\Delta\phi, \Delta w)$ phase plane and the longitudinal beam emittance at linac input Uniform transverse density distribution in unbunched beam.

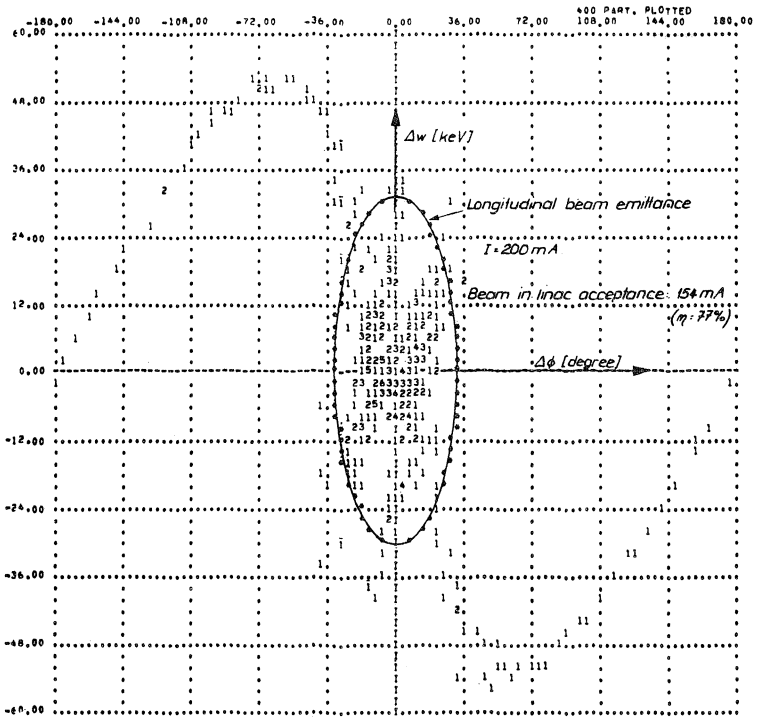

Fig. 11c : Same as 11a, but with truncated gaussian density distribution

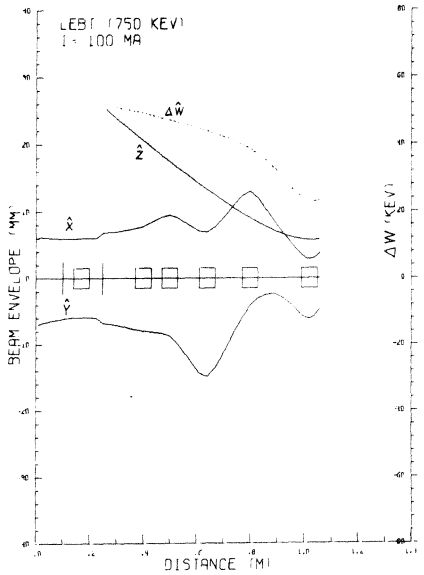

Fig. 12a: Transport of a 100 mA beam through the bunching section; third buncher off (parabolic density distribution in unbunched beam.)

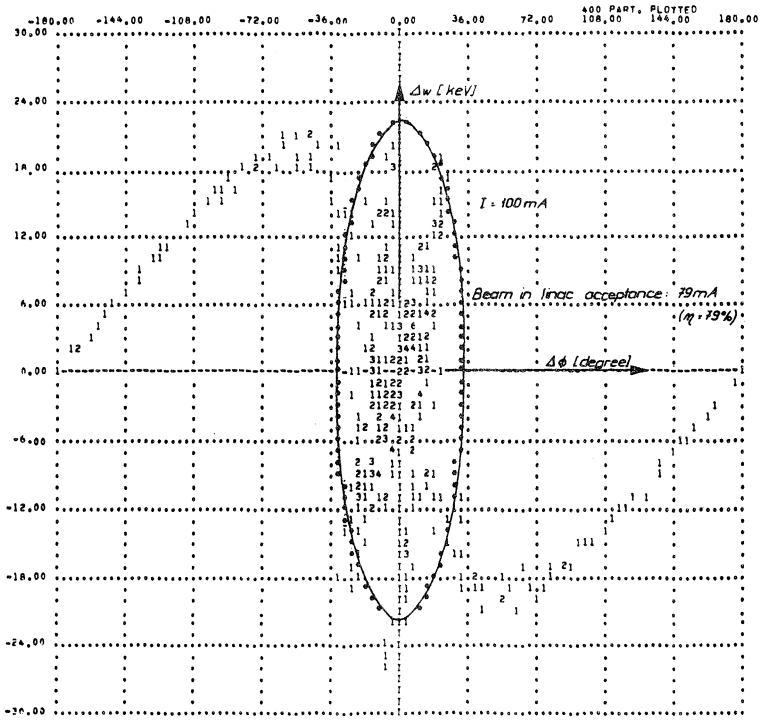

Fig. 12b: Scatter diagram in $(\Delta\phi, \Delta w)$ phase plane at linac input

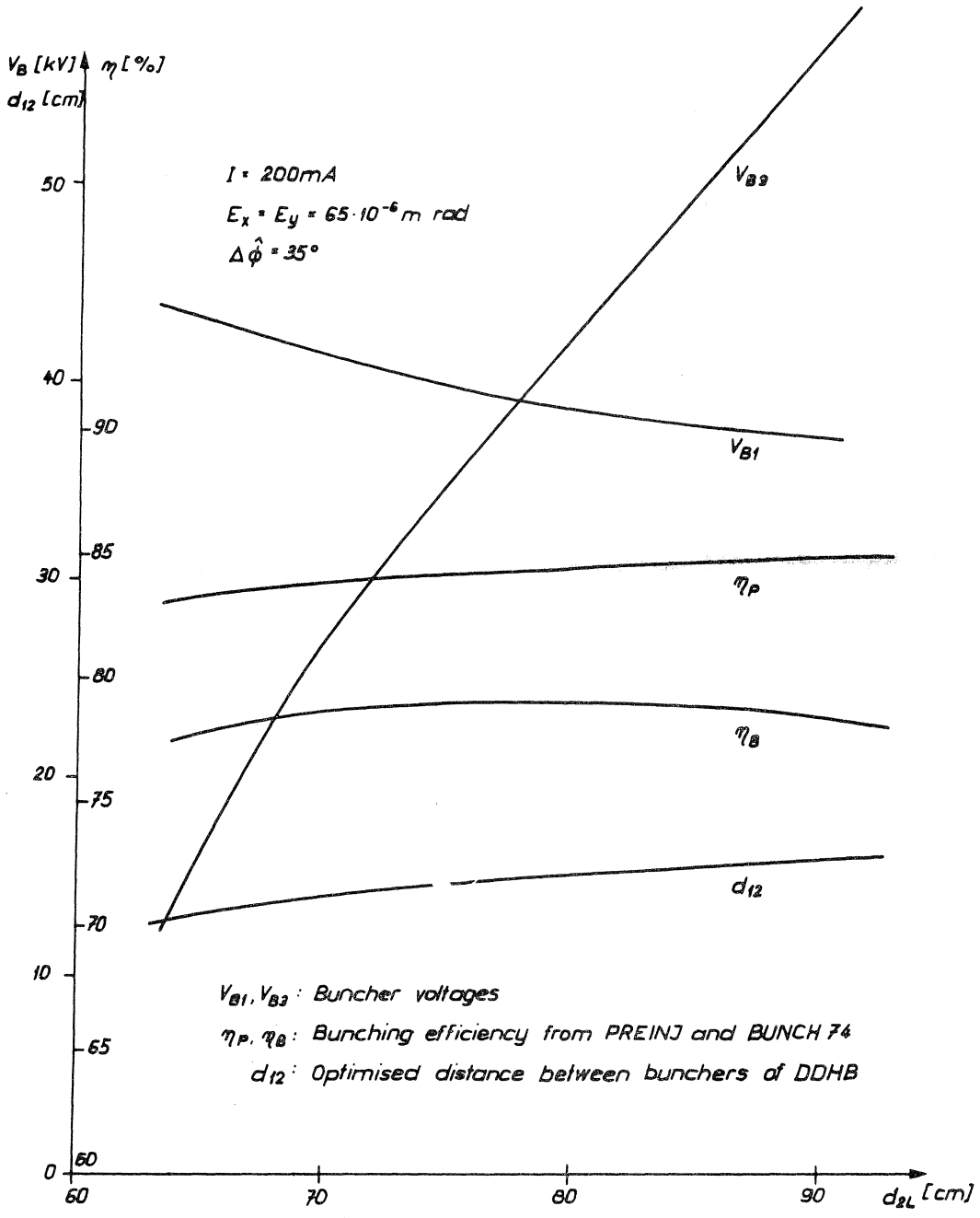

Fig. 13: Parameters of the bunching system as function of d_{2L} (d_{2L} ... distance of 2nd harmonic buncher to Linac input plane)

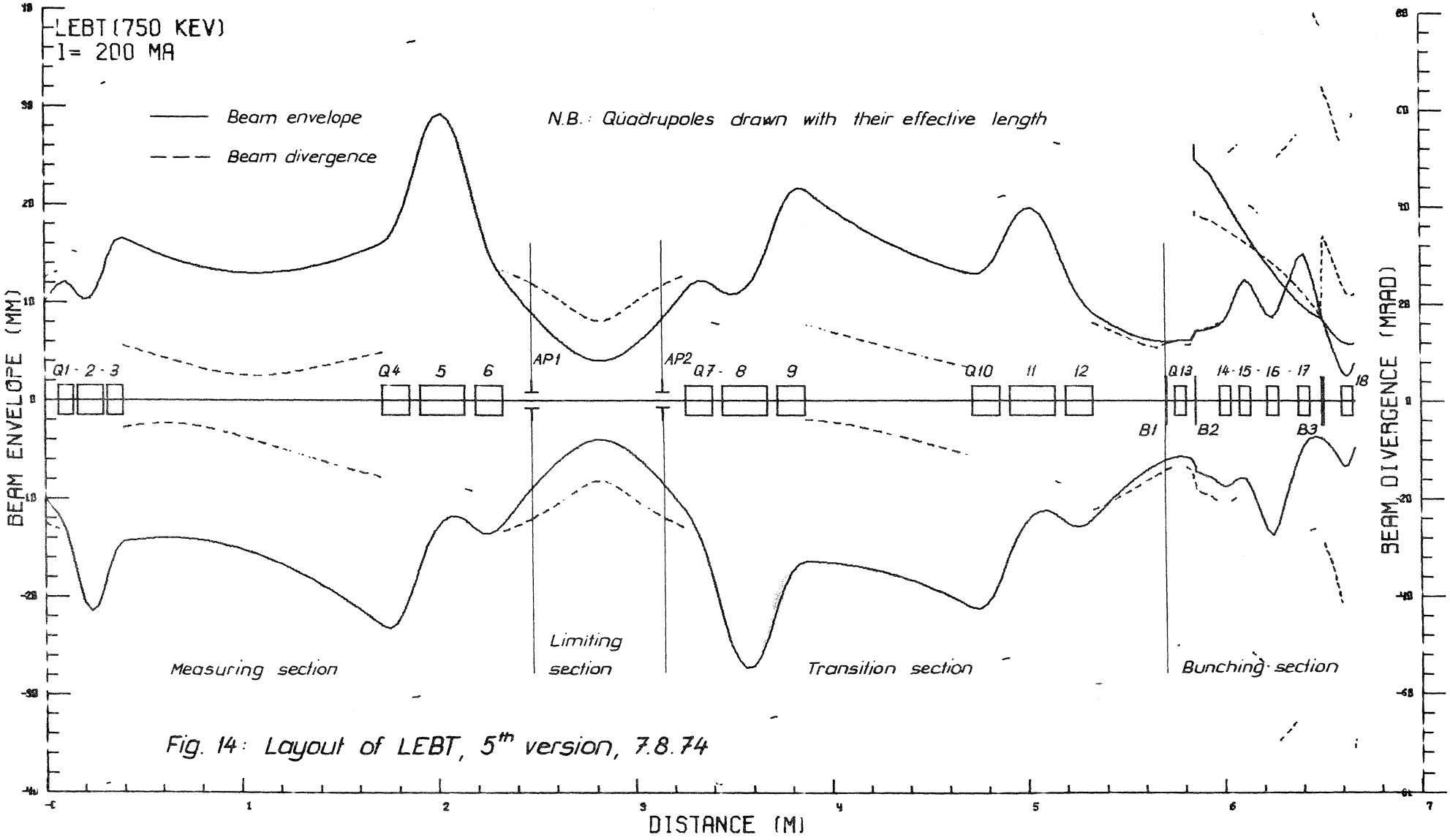

Fig. 14: Layout of LEBT, 5th version, 7.8.74

Input Conditions (preaccelerator beam characteristics)

I_p = 200 mA (nominal)

E = 65 10^{-6} m rad; E_{rms} = 16.25 10^{-6} m rad

beam envelope : $\hat{x} = \hat{y}$ = 10 mm; $\tilde{x} = \tilde{y}$ = 5 mm

beam divergence : $\hat{x}' = \hat{y}'$ = 25 10^{-3} rad; $\tilde{x}' = \tilde{y}'$ = 12.5 10^{-3} rad

---

Output conditions (end of 1st half drift tube in tank I)

$\frac{\overline{xx'}}{E_{xrms}}$ = 2.23	horizontal plane
$\frac{\overline{x^2}}{E_{xrms}}$ = 0.16 m	
$\frac{\overline{yy'}}{E_{yrms}}$ = -3.22	vertical plane
$\frac{\overline{y^2}}{E_{yrms}}$ = 0.24 m	
$\Delta\Phi$ = 35°	longitudinal plane
ΔW = 33.2 keV	
$\frac{\overline{\Delta\Phi\Delta W}}{E_{\Phi rms}}$ = 0.28	

Quadrupoles and bunchers

	Quad. Identif.	Length (mm)	Aperture (mm)	Gradient (T/m) I = 200 mA
Measuring section (2.483 m)	Q1, Q3	60	70	- 7.3
	Q2	120	70	7.7
	Q4, Q6	100	100	3.1
	Q5	190	100	- 3.1
Beam limiting section (0.675 m)				
Transition section (2,548 m)	Q7, Q9	100	100	- 3.1
	Q8	190	100	3.1
	Q10, Q12	100	100	2.8
	Q11	190	100	- 2.8
Bunching section (0.948 m)	Q13	45	30	- 2.7
	Q14	50	50	9.1
	Q15	50	50	-16
	Q16	50	50	19.4
	Q17	50	50	-19.6
	Q18	45	30	39.8
Buncher voltages (kV) : V_{B1} = 52.6; V_{B2} = 44; B_{B3} = 58				

Length of LEBT : 6.654 m

FIGURE 15 : Focusing parameters of LEBT (5th version, 7.8.74)

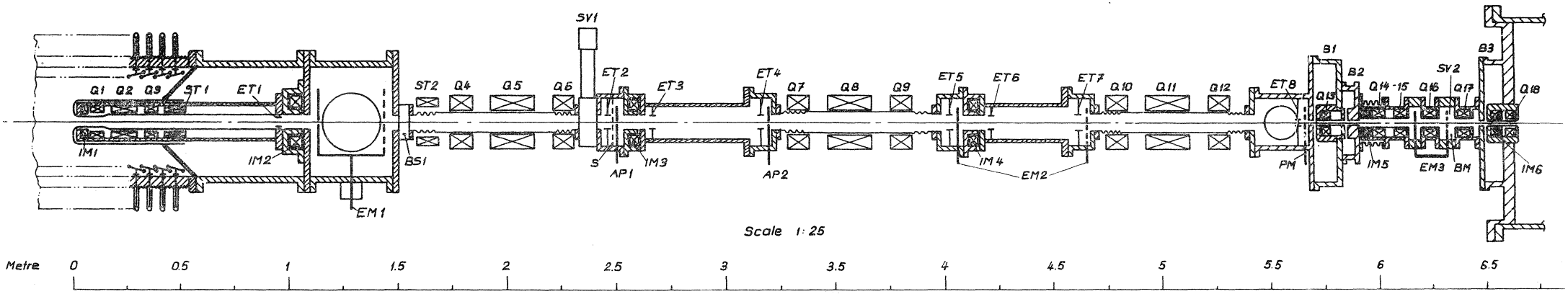

Q = Quadrupole
ST = Steering coil
B = Buncher
ET = Electron trap

IM = Beam transformer
EM = Emittance meas. device
PM = Beam profile meas. device
BM = Bunch profile meas. device

S = Sieve
AP = 4-jaw aperture
BS = Beam stopper
SV = Sector valve

Fig. 16: Schematic drawing of LEBT

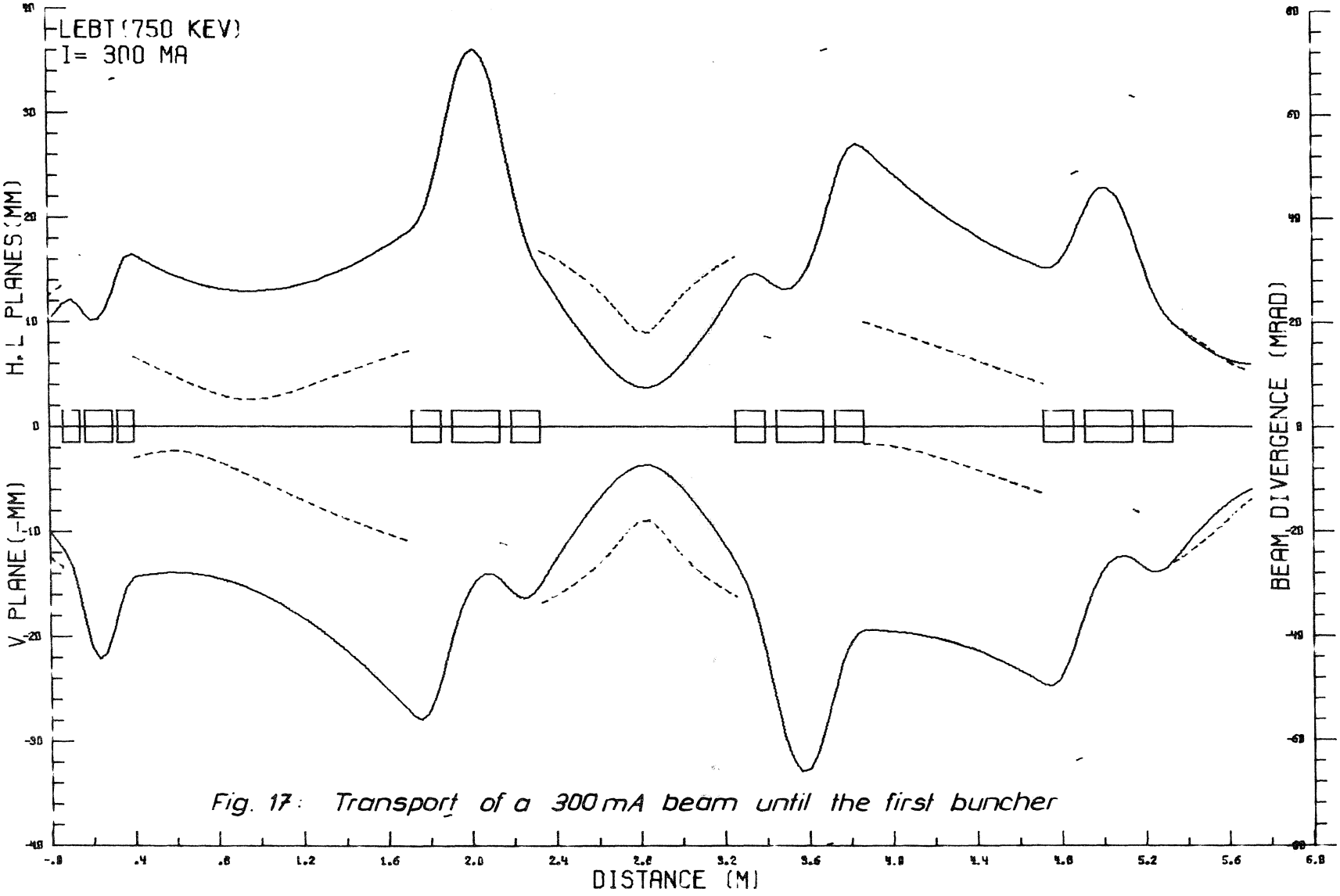

Fig. 17 : Transport of a 300 mA beam until the first buncher

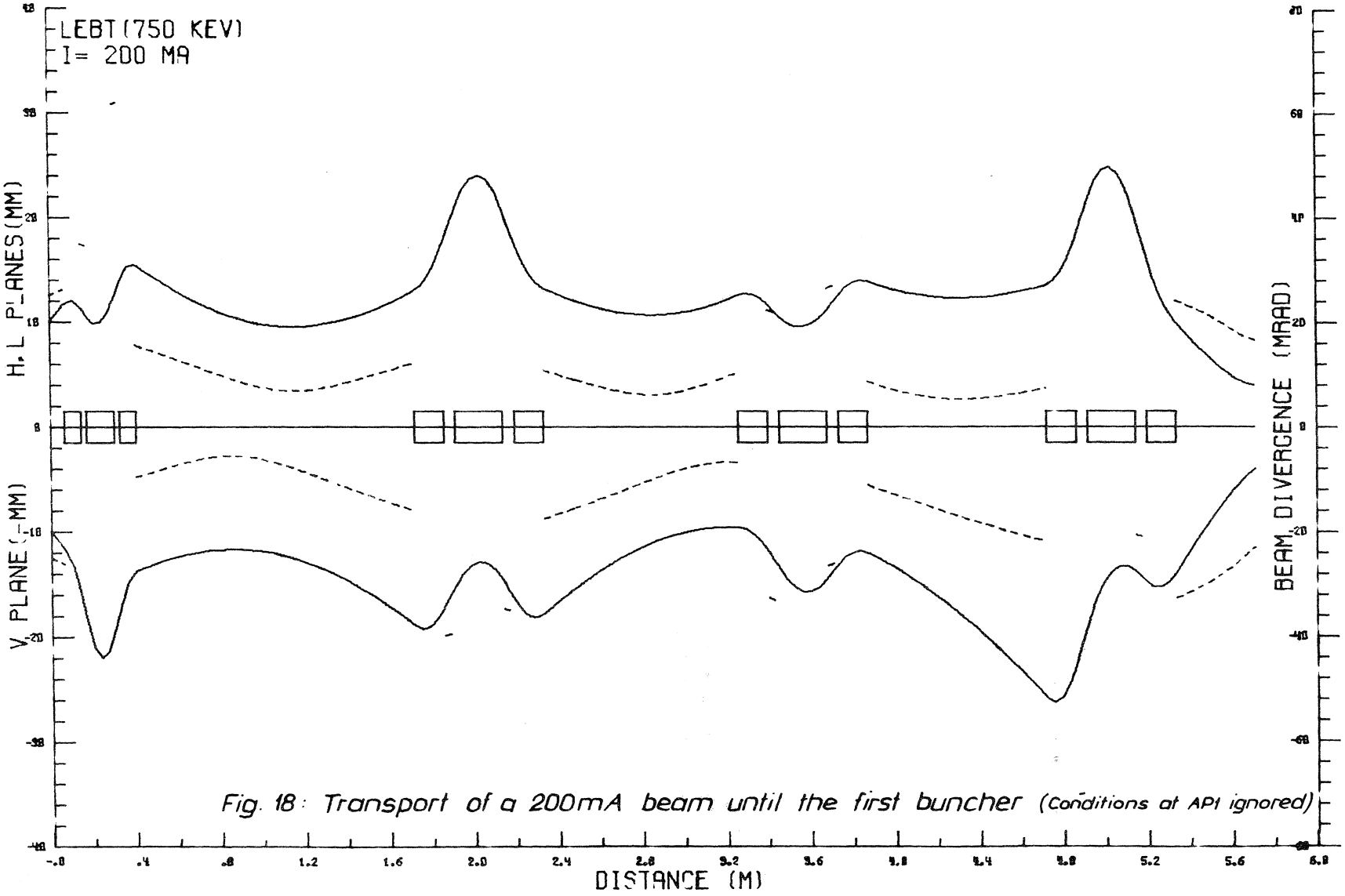

Fig. 18 : Transport of a 200mA beam until the first buncher (conditions at API ignored)

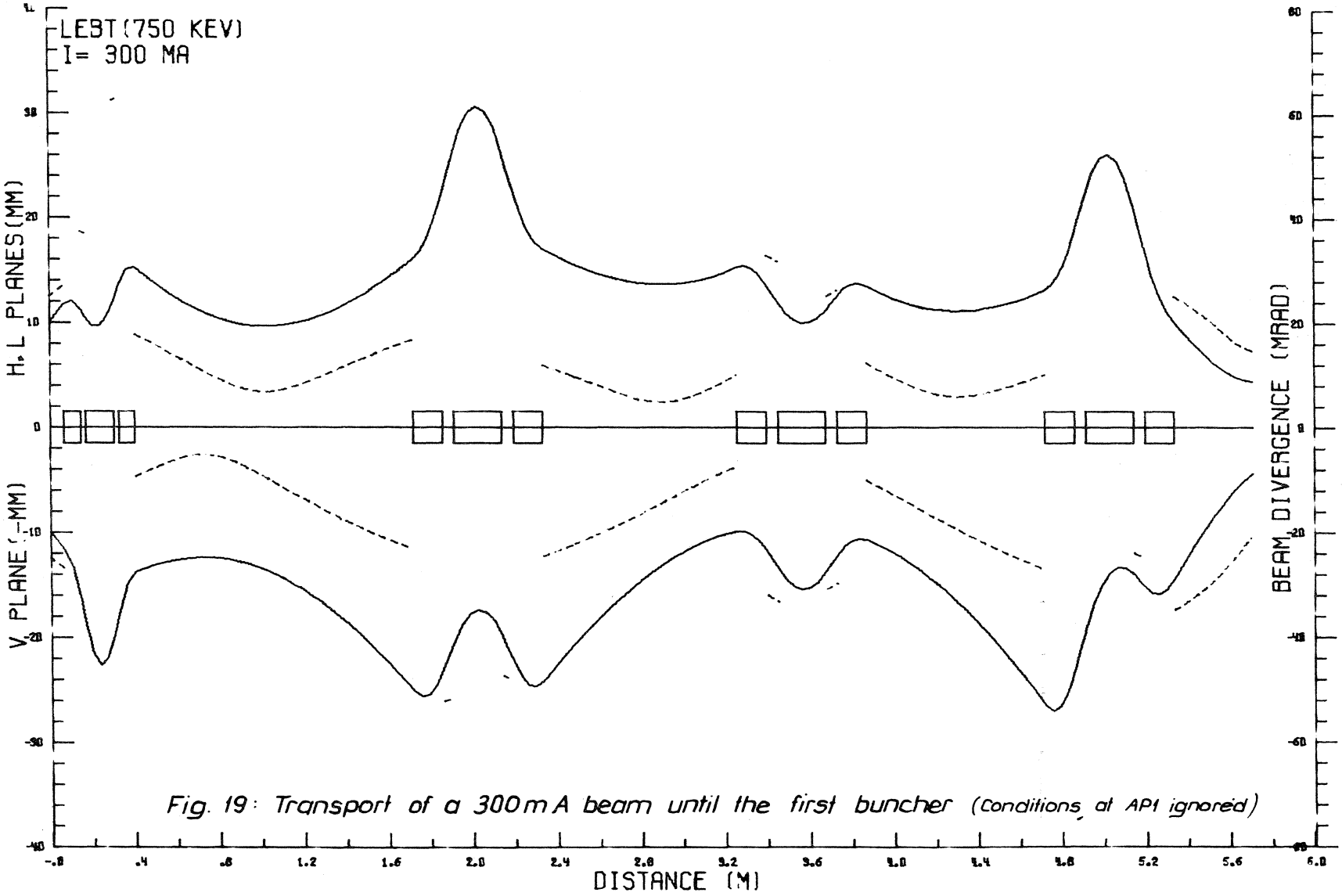

Fig. 19: Transport of a 300 mA beam until the first buncher (Conditions at AP1 ignored)

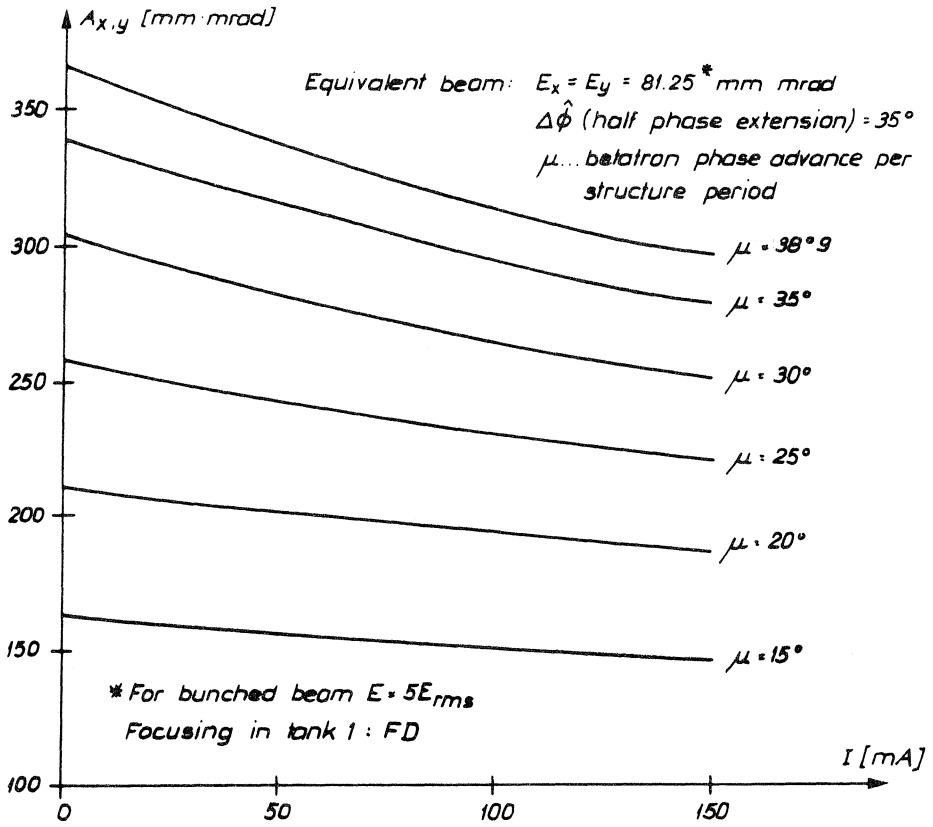

Fig. 20a : Transverse linac acceptance for nominal accelerating conditions in tank 1

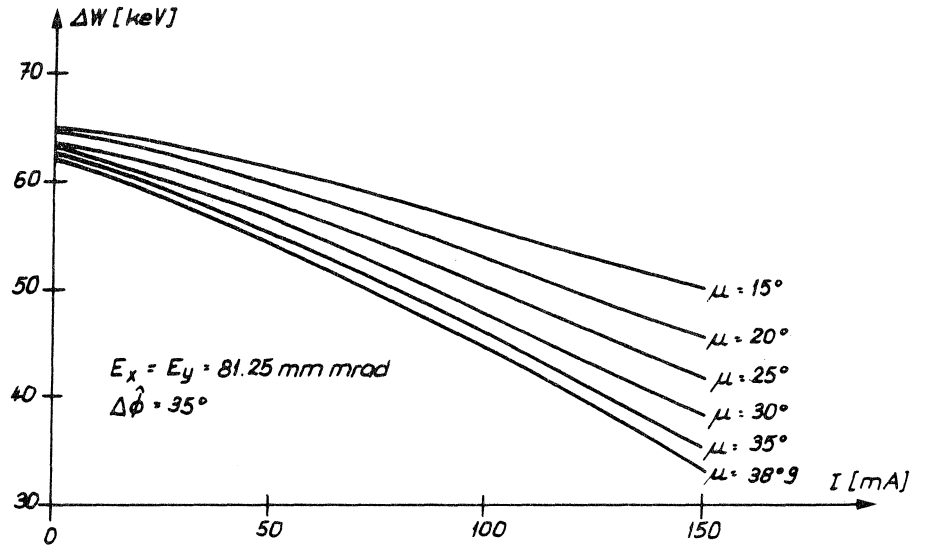

Fig. 20b: Energy spread of matched beam at linac input (end of 1st half drift tube)

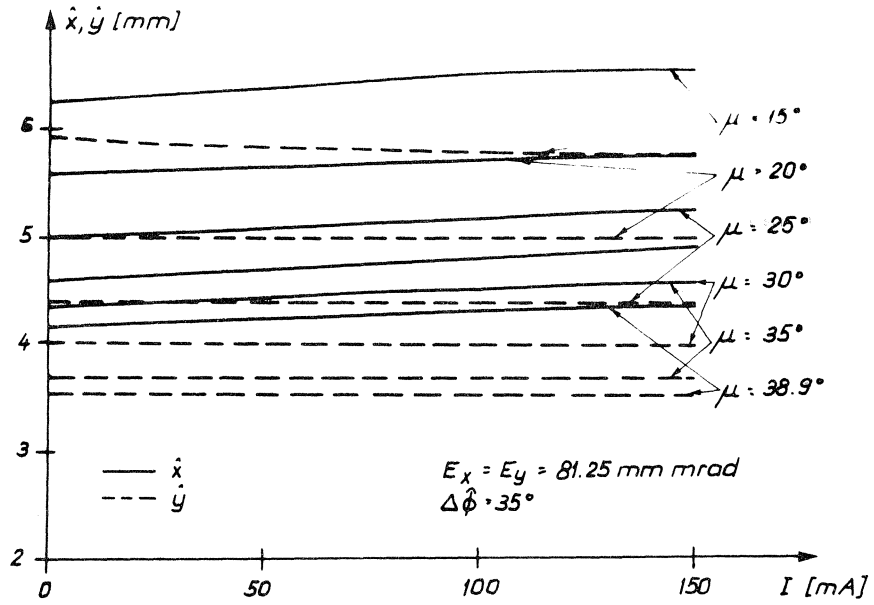

Fig. 21a: Matched beam envelopes at linac input

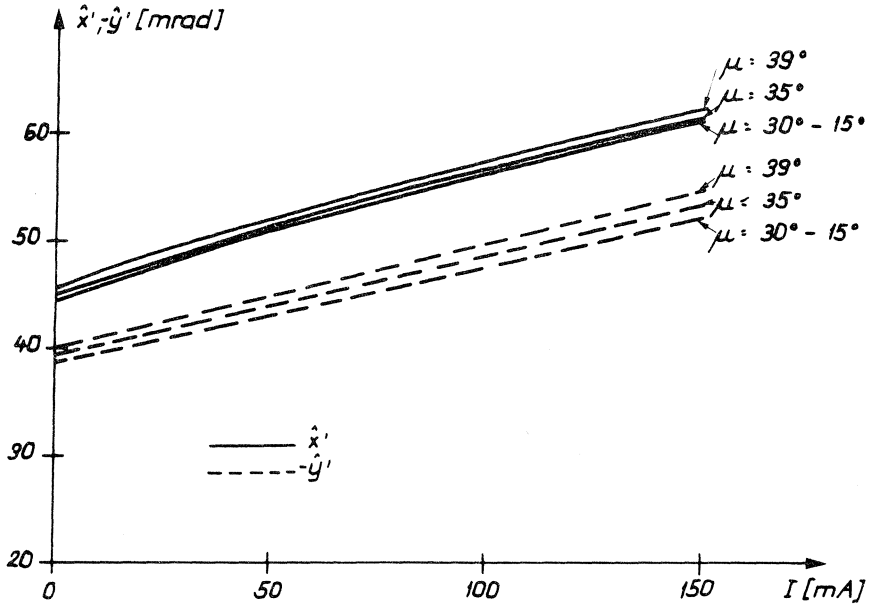

Fig. 21b: Matched beam divergences at linac input

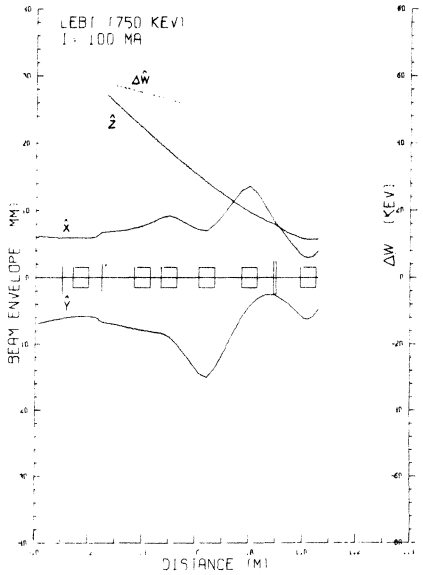

Fig. 22a: Transport of a 100 mA beam through the bunching section (parabolic density distribution)

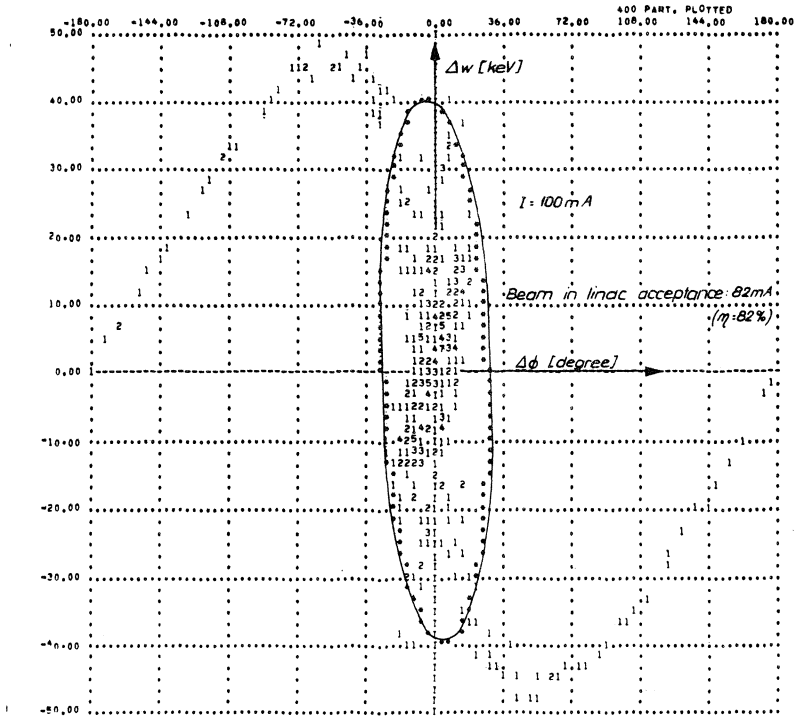

Fig. 22b: Scatter diagram in (Δφ, Δw) phase plane at linac input

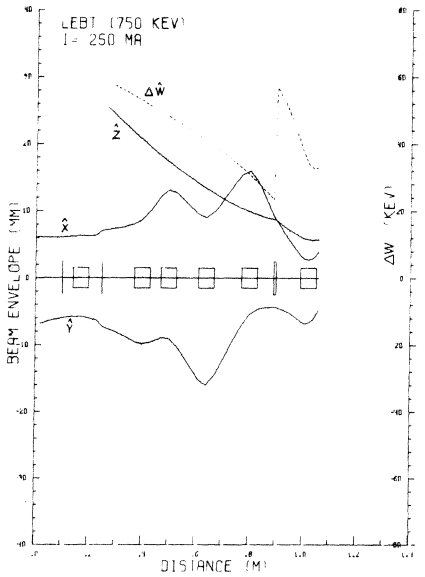

Fig. 23a: Transport of a 250mA beam through the bunching section (parabolic density distribution)

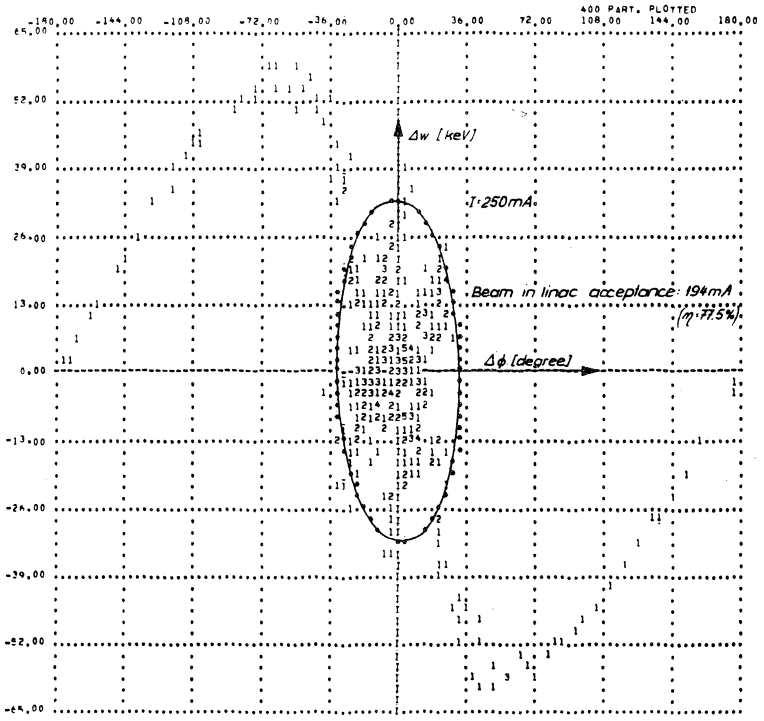

Fig. 23b: Scatter diagram in (Δφ, Δw) phase plane at linac input

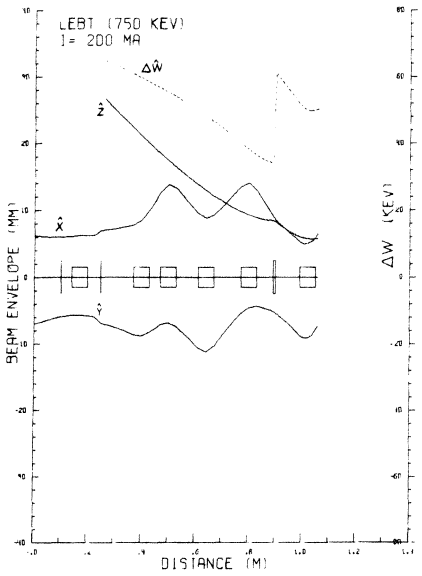

Fig. 24a: Transport of a 200mA beam through the bunching section and matching to linac which is operating with $\mu = 15°$ (parabolic density distribution)

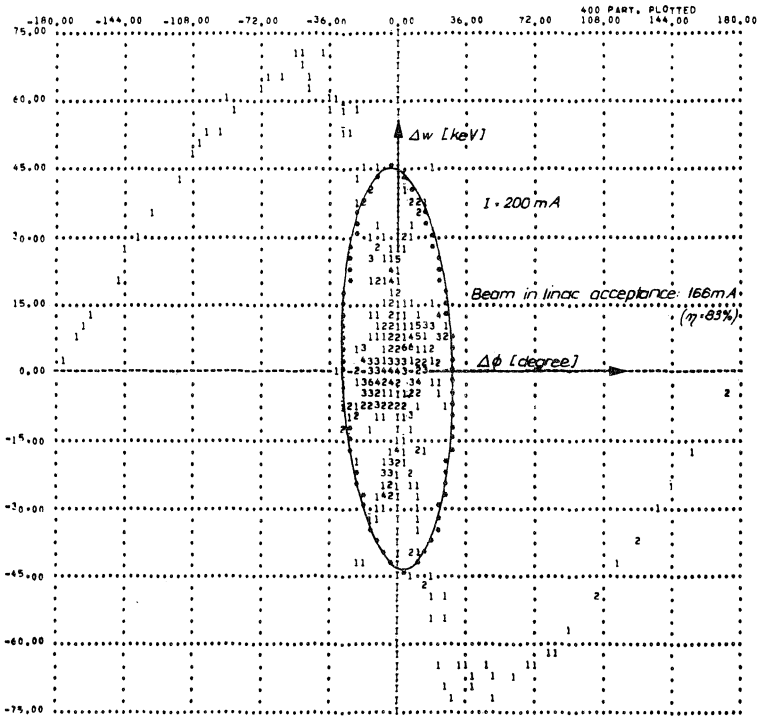

Fig. 24b: Scatter diagram in $(\Delta\phi, \Delta w)$ phase plane at linac input

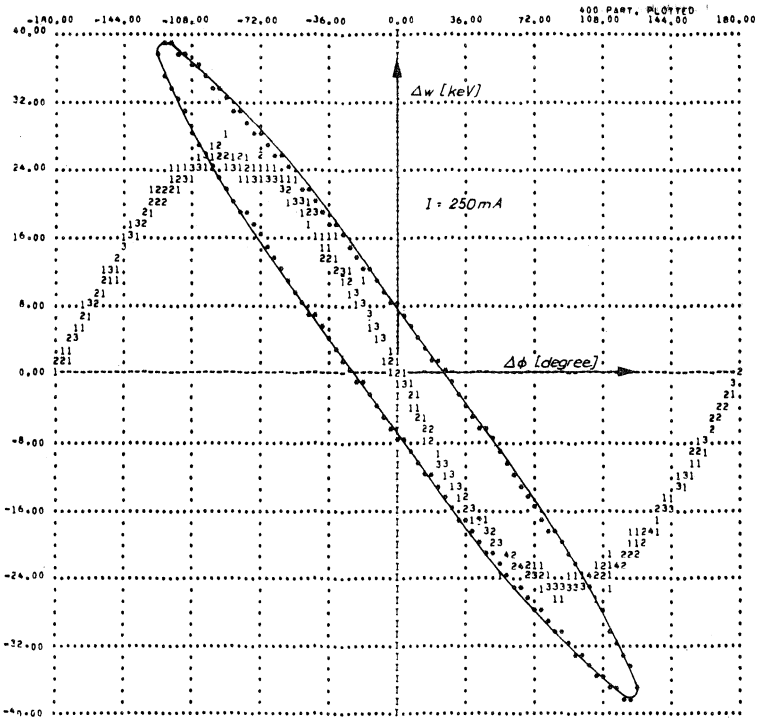

Fig. 25: Scatter diagram in the $(\Delta\phi, \Delta w)$ phase plane at the 1st buncher, for $I = 250\,mA$ (parabolic density distribution); 2nd buncher (harmonic) off.

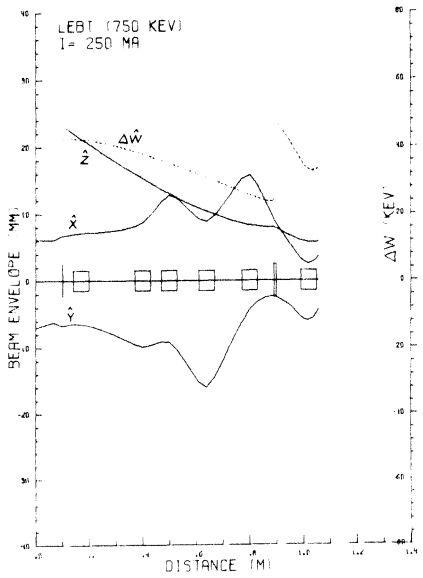

Fig. 26a: Transport of a 250 mA beam through the bunching section with the 2nd harmonic buncher off

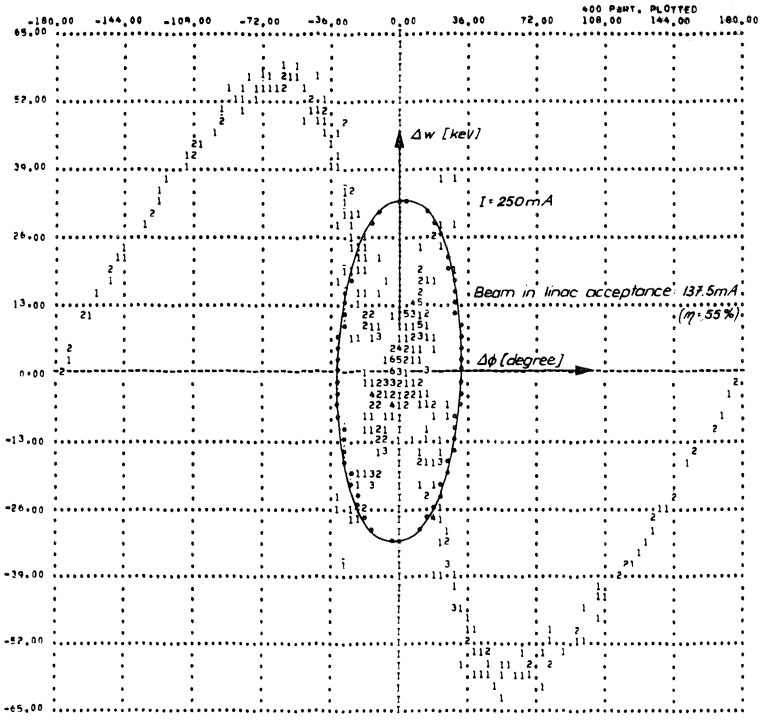

Fig. 26b: Scatter diagram in the ($\Delta\phi$, Δw) phase plane at linac input